Neural circuit mechanisms for transforming learned olfactory valences into wind-oriented movement

Yoshinori Aso[1]*, Daichi Yamada[2], Daniel Bushey[1], Karen Hibbard[1], Megan Sammons[1], Hideo Otsuna[1], Yichun Shuai[1], Toshihide Hige[2,3,4]*

1: Janelia Research Campus, Howard Hughes Medical Institute, Ashburn, United States

2: Department of Biology, University of North Carolina at Chapel Hill, Chapel Hill, United States

3: Department of Cell Biology and Physiology, University of North Carolina at Chapel Hill, Chapel Hill, United States

4: Integrative Program for Biological and Genome Sciences, University of North Carolina at Chapel Hill, Chapel Hill, United States

Contact Info

asoy@janelia.hhmi.org

hige@email.unc.edu

Summary

How memories are used by the brain to guide future action is poorly understood. In olfactory associative learning in Drosophila, multiple compartments of the mushroom body act in parallel to assign valence to a stimulus. Here, we show that appetitive memories stored in different compartments induce different levels of upwind locomotion. Using a photoactivation screen of a new collection of split-GAL4 drivers and EM connectomics, we identified a cluster of neurons postsynaptic to the mushroom body output neurons (MBONs) that can trigger robust upwind steering. These UpWind Neurons (UpWiNs) integrate inhibitory and excitatory synaptic inputs from MBONs of appetitive and aversive memory compartments, respectively. After training, disinhibition from the appetitive-memory MBONs enhances the response of UpWiNs to reward-predicting odors. Blocking UpWiNs impaired appetitive memory and reduced upwind locomotion during retrieval. Photoactivation of UpWiNs also increased the chance of returning to a location where activation was initiated, suggesting an additional role in olfactory navigation. Thus, our results provide insight into how learned abstract valences are gradually transformed into concrete memory-driven actions through divergent and convergent networks, a neuronal architecture that is commonly found in the vertebrate and invertebrate brains.

Introduction

Animals assign a valence to a stimulus based on experience. Such learning events induce an enduring modification in the stimulus-evoked activity of the nervous system and ultimately change the behavioral response to future encounters with the same stimulus. In mammals, the amygdala is the primary site for valence assignment during Pavlovian learning (O'Neill et al., 2018). As a neutral sensory stimulus (conditioned stimulus, CS) is paired with punishment or reward (unconditioned stimulus, US), the CS

acquires the capacity to evoke valence-specific response patterns in the amygdala (Grewe et al., 2017; Zhang and Li, 2018). However, the circuit process in which these learning-dependent CS representations lead to concrete motor patterns during memory retrieval is poorly understood. Comprehensive understanding of this process requires detailed knowledge of the downstream connectivity of the plastic CS-representing neurons. Nevertheless, it has been shown that amygdala-dependent valence-specific behaviors are mediated by distinct networks (Gore et al., 2015) whose outputs diverge to different projection areas responsible for aversive or appetitive unconditioned responses (Beyeler et al., 2016; Namburi et al., 2015). There is also evidence for an alternative mechanism where neurons capable of eliciting opposing behaviors converge on the same target areas or neurons. For example, GABAergic and glutamatergic projection neurons from the lateral hypothalamus to the ventral tegmental areas (VTA) can evoke appetitive and aversive behaviors, respectively. These projection neurons converge on the same population of GABAergic neurons in VTA to differentially control downstream dopaminergic neurons (Nieh et al., 2016). Thus, both divergent and convergent circuit motifs are considered important for the valence-to-behavior transformation in vertebrates (Tye, 2018).

Divergent pathways for valence processing are also evident in the memory circuit in Drosophila both anatomically and functionally. In fly olfactory learning, the primary site for CS-US association is the mushroom body (MB), where parallel axon fibers of the odor-encoding Kenyon cells (KCs) are segmented into a series of MB compartments that are defined by the dendrites of MB output neurons (MBONs) andaxons of US-encoding dopaminergic neurons (DANs) (Aso et al., 2014a; Tanaka et al., 2008)(Figure 1A). While population activity of KCs represents odor identity (Campbell et al., 2013), that of MBONs is less effective in doing so (Hige et al., 2015b). Instead, individual MBONs are

70 considered to encode the valence of stimuli because optogenetic activation of each type
71 of MBONs can elicit either approach or avoidance behavior (Aso et al., 2014b; Owald et
72 al., 2015). However, MBONs do not appear to command specific motor sequences
73 because their activation does not induce stereotyped motor patterns (Aso et al., 2014b).
74 Thus, how abstract valence signals carried by MBONs are translated into concrete motor
75 patterns is unknown.
76
77 The MB compartments are arranged such that the valence of DANs is opposite to that of
78 the corresponding MBONs in a given compartment (Aso et al., 2014b). During learning,
79 coactivation of DANs and KCs induces long-term depression of KC-MBON synapses in
80 a compartment-specific manner (Berry et al., 2018; Cohn et al., 2015; Hige et al., 2015a;
81 Owald et al., 2015). Thus, the prevailing hypothesis is that learning-induced depression
82 in a subset of MBONs tips the collective balance of positive and negative valences
83 represented by the MBON population, which are in balance in naive flies, and thereby
84 biases the odor choice (Heisenberg, 2003; Hige, 2018; Modi et al., 2020; Owald and
85 Waddell, 2015). Supporting this view, photoactivation of multiple types of MBONs
86 encoding the same or opposite valences exerts additive effects for induction of attraction
87 and avoidance (Aso et al., 2014b). This model predicts that the circuits downstream of
88 the MB should be sensitive to skewed activity patterns of the MBON population. Such a
89 computation can be performed by neurons integrating or comparing the output signals of
90 multiple MBONs. In fact, axon terminals of the MBONs are confined to relatively limited
91 brain regions, suggesting that they converge on common neurons (Aso et al., 2014a).
92 The comprehensive EM connectome indeed revealed that 600 out of 1550 postsynaptic
93 neurons of MBONs also receive input from at least one other MBON (Li et al., 2020).
94 However, whether those convergent circuit motifs function to decode the parallel

memories formed in the MB and, if so, how they shape motor patterns during memory retrieval are unknown.

The functional diversity of the MB compartments is not limited to the sign of memory valence. At least 5 out of 15 MB compartments are identified as appetitive memory compartments, and yet they exhibit distinct memory properties (Aso et al., 2014b; Aso and Rubin, 2016). For example, memory formation in the α1 compartment requires relatively long training, but once formed, lasts more than a day. In contrast, memory in γ5β′2a requires only a single training to form but is transient and easily overwritten by the subsequent training (Aso and Rubin, 2016; Ichinose et al., 2021; Yamada et al., n.d.). Compartments are also tuned to distinct types of reward. While α1 memory is essential for nutritional value learning (Yamagata et al., 2015), γ4 and β′2 compartments function in water reward learning (Lin et al., 2014). Despite this diversity, memory formation in any appetitive compartments can promote attraction to the associated odor. The behavioral strategies used to find the source of attractive odors are not analyzed in typical olfactory learning assays (Tully and Quinn, 1985), that measure the relative distributions of flies between learned and control odors. Thus, the roles played by individual appetitive memory compartments in guiding approach to an attractive odor remain unknown.

By analyzing walking trajectories of individual flies, we found that appetitive memories formed in the α1 compartment are able to bias the turning direction so that a fly move upwind. By photoactivation screening, we identified a single cluster of neurons, UpWiNs, that can promote robust upwind steering and acceleration of locomotion. UpWiNs receive inputs from several types of lateral horn neurons and integrate inhibitory and excitatory inputs from MBON-α1 and MBON-α3, which are the MBONs that convey long-

term appetitive or aversive memories, respectively. UpWiNs enhance responses to odors after induction of memory in the α1, and the activity of UpWiNs is required for appetitive memory and memory-driven upwind locomotion. Taken together, our work provides important insights into the process of valence integration, which we show employs a convergent circuit motif commonly found downstream of memory centers, and reveals circuit mechanisms that underlie the gradual transformation from abstract valence to specific motor commands.

Results

Identification of the MB compartments that drive upwind locomotion

To analyze behavioral components of memory-driven odor response, we used a modified four-armed olfactory arena in which odors are delivered through the current of airflow from the four channels at corners to the suction tubing at the center (Figure 1B) (Aso and Rubin, 2016; Pettersson, 1970; Vet et al., 1983). The airstream from each channel forms sharp boundaries at the border of quadrants. Each of four quadrants can be filled with an arbitrary odor, but we typically used it either for presentation of a single odor in all quadrants or for binary choice by presenting two odors in diagonal quadrants (Figure 1C).

To test whether appetitive olfactory memories created in different MB compartments elicit distinct behaviors during memory retrieval, we first trained flies by pairing an odor as the CS+ with optogenetic activation of one of four sets of DANs. Each set of DANs projects to distinct appetitive memory compartments: γ5β′2a, γ4, β1β2 or α1 (Huetteroth et al., 2015; Ichinose et al., 2015; Lin et al., 2014; Liu et al., 2012; Yamagata et al., 2015). A second odor was presented without DAN activation as CS- (Figures 1C). These optogenetic activations promoted local release of dopamine in the targeted MB compartments (Sun et al., 2020; Yamada et al., n.d.). We used a pair of odors, Pentyl Acetate (PA) and Ethyl Lactate (EL), that evokes activity in discrete sets of KCs (Campbell

147 et al., 2013). After three training sessions, flies exhibited strong preference to the CS+
148 odor when given a choice between CS+ and CS- odors (Figure 1D). Next, we asked if
149 these MB-compartment-specific memories can drive wind-directed movement when CS+
150 or CS- odors were presented separately for 10 seconds (Figure 1C). We measured the
151 movement of individual flies and their heading angle relative to the upwind direction and
152 analyzed how those parameters changed in response to odors. Despite robust CS+
153 preference in a binary choice, memories in the γ5β′2a and the γ4 failed to promote
154 significant upwind movement (Figure 1E-F). In contrast, memories in the α1 and the β1β2
155 promoted steering and walking upwind in response to the CS+ odor, compared to genetic
156 controls and the "No LED" control group of the same genotype (Figure 1E-F). The memory
157 in the α1 compartment also reduced upwind locomotion in response to CS- odor compared
158 to the genetic control groups. These initial analyses compared averages of all ~20 flies in
159 each movie. By separately analyzing behaviors of individual flies based on their orientation
160 at the onset of odors, we found that memories in the α1 and β1β2 biased the direction of
161 turning to steer toward upwind (Figure 1 G). Memories in γ5β′2a and γ4 did not bias the
162 turning direction, although they promoted flies facing downwind to change orientation in a
163 non-directional manner (Figure 1G and Figure 1-figure supplement 1). These results
164 indicate that appetitive memory retrieval involves distinct behavioral strategies depending
165 on the localization of the memory in the MB. Specifically, MBONs from the α1 and the
166 β1β2 compartments, but not those from γ5β′2a or γ4, appear to be connected to circuit
167 components that drive memory-driven upwind steering.
168

169 **Identification of UpWind Neurons by optogenetic screening**

170 We next set out to identify the circuit elements that function downstream of the MBONs to
171 induce memory-driven, wind-guided locomotion. To enable cell-type-specific experimental
172 manipulation, we have made a large collection of split-GAL4 drivers. Using a subset of

173 these lines, we conducted optogenetic screening to test if activation of certain neurons
174 can promote wind-directed movement. We analyzed how starved flies respond to 10s
175 optogenetic stimulation of various cell types in the circular arena with airflow but no
176 olfactory stimuli (Figure 2). We measured the changes in the fly's distance from the center,
177 heading angle relative to the upwind direction, angular velocity and walking speed.
178 Because returning to the odor plume is a major component of olfactory navigation (Baker,
179 1990; Cardé, 2021), we also measured the probability of a fly returning to its starting
180 location after moving away.

181 Although our screen is not comprehensive in terms of the coverage of the cell types
182 or brain areas, it successfully identified several clear "hits", which include both known and
183 previously uncharacterized cell types. Most of the lines with phenotypes showed increased
184 upwind locomotion, but we did find four lines, which label SMP120/124, MBON01/03/04
185 or CRE039, that promoted locomotion in the downwind direction (Figure 2 and Figure 2-
186 figure supplement 1 and 2). As previously reported (Matheson et al., 2022), activation of
187 some MBON types including MBON-α3 (also known as MBON14 or MBON-V3) and
188 MBON-γ2α′1 (MBON12) promoted significant upwind locomotion. Figure 2B summarizes
189 the detailed time courses of these behavioral phenotypes before, during and after 10s
190 LED stimulations. These behavioral data can be immediately put into the context of the
191 EM connectome map, since the cell types in each driver lines were morphologically
192 matched by comparing confocal and electron microscope images (see examples in Figure
193 2-figure supplement 2 and 3).

194 Among the split-GAL4 drivers we screened, SS33917 and SS33918 showed the
195 strongest upwind locomotion, especially at the onset of 10s activation period (Figure 2B
196 and Figure 2-figure supplement 1). These driver lines label a similar set of 8-11 neurons
197 (Figure 2-figure supplement 2). Here, we will focus our analysis on this cluster of neurons,

198 which we collectively call UpWind Neurons (UpWiNs), based on their robust activation
199 phenotype and anatomical connections with the α1 compartment (see below).
200
201 **UpWiNs integrate inputs from MBONs**
202 The UpWiNs have extensive arborizations in the dorsolateral area of the brain where
203 MBON-α1 (also known as MBON07) and MBON-α3 send converging axons (Video 1 and
204 2; Figure 3A). The α1 and α3 compartments store appetitive and aversive long-term
205 memories, respectively (Aso and Rubin, 2016; Huetteroth et al., 2015; Ichinose et al.,
206 2015; Jacob and Waddell, 2022; Matheson et al., 2022; Pai et al., 2013; Yamagata et al.,
207 2015). DANs innervating the α1 and α3 compartments respond to sugar or electric
208 shock/heat/bitter, respectively (Jacob and Waddell, 2022; Kirkhart and Scott, 2015;
209 Schnitzer et al., n.d.; Siju et al., 2020; Yamagata et al., 2015). MBON-α1 displays reduced
210 odor response to an odor associated with activation of DANs in α1 (Yamada et al., n.d.),
211 whereas MBON-α3 increases response to an odor associated with sugar reward possibly
212 due to interactions with appetitive memory compartments such as the β1 (Li et al., 2020;
213 Plaçais et al., 2013; Takemura et al., 2017; Tanaka et al., 2008) and decreases response
214 to punishment-associated odors (Jacob and Waddell, 2022; Schnitzer et al., n.d.). Both
215 MBONs are required for retrieval of long-term appetitive memory (Ichinose et al., 2015;
216 Plaçais et al., 2013). These previous reports raise the possibility that the UpWiNs defined
217 by the SS33917 driver might play a role in both the upwind locomotion observed during
218 retrieval of an α1 memory (Figure 1) and the activation of MBON-α3 (Matheson et al.,
219 2022)(MB082C data in Figure 2).
220 To test this possibility, we first examined the anatomical connectivity of the UpWiNs. We
221 obtained images of 25 individual neurons in SS33917-split-GAL4 by the multi-color flip-
222 out method and compared them with reconstructed EM-images (Figure 3 and Figure 3
223 supplement 1-3) (Nern et al., 2015; Otsuna et al., n.d.; Scheffer et al., 2020). This analysis

224 identified eleven neurons of five cell types in the hemibrain EM dataset as UpWiN neurons
225 (Figure 3 Figure supplement 1 and 2). Among 11 matched EM-reconstructed neurons of
226 the UpWiNs, four neurons, one SMP353 and three SMP354 neurons, receive direct
227 synaptic input from MBON-α1 (Figure 3B-E)(Li et al., 2020; Scheffer et al., 2020). SMP354
228 also receives input from MBON-α3; this strong convergent connectivity is exceptional
229 among the population of the neurons that are postsynaptic to either of the MBONs (Figure
230 3D and Figure 3-figure supplement 4). The rest of the UpWiNs do not have direct
231 connections with these MBONs, but receive indirect input from them (see Figure 3F). The
232 excitatory interconnections within the UpWiN cluster suggests that these neurons may
233 function as a group, even though the connectivity of the individual neurons is
234 heterogeneous. Interestingly, all the UpWiNs provide input to a single neuron, SMP108
235 (Figure 3C), which has the highest number of connections with reward DANs and plays a
236 key role in second-order conditioning (Yamada et al., n.d.). The axon terminals of UpWiNs
237 are immunoreactive to choline acetyltransferase (Yamada et al., n.d.), and therefore likely
238 to be excitatory to the SMP108 and other downstream neurons. The SMP108 is labeled
239 in SS45234 and SS67221, and its activation also promoted upwind locomotion (Figure 2;
240 Figure 2-figure supplement 1).
241
242 To test functional connectivity, we made in vivo whole-cell recordings from
243 UpWiNs, while optogenetically activating either MBON-α3 or MBON-α1. Neurons were
244 randomly targeted by the electrode among those labeled by R64A11-LexA, which is a
245 broad driver for UpWiNs. R64A11 is a hemi-driver for the DNA-binding domain of the
246 SS33917-split-GAL4. A brief 10 ms stimulation of cholinergic MBON-α3 evoked a strong
247 excitation in 2 out of 6 UpWiNs examined, whereas glutamatergic MBON-α1 evoked
248 inhibitory responses in 4 out of 17 UpWiNs (Figure 4A-B). The observed stochasticity of
249 the connectivity is consistent with the EM connectome data. Postsynaptic sites of MBON-

250 α1 and MBON-α3 are juxtaposed on the dendrites of UpWiNs (Figure 3E), implying
251 dendritic integration of these inputs. Since we did not have a LexA driver that selectively
252 labels SMP354, we were unable to specifically target those integrating UpWiNs by
253 electrophysiology. We therefore measured the population activity of UpWiNs at the
254 junction between their dendrites and proximal axons by two-photon calcium imaging in
255 dissected brains. Consistent with the electrophysiological results and the circuit model, we
256 observed a calcium increase upon MBON-α3 activation. Moreover, MBON-α1 activation
257 suppressed the excitatory effect of MBON-α3 when they were activated together (Figure
258 4C). These results indicate that UpWiNs receive and integrate synaptic inputs from
259 MBONs that signal opposite signs of memory valence.
260
261 **UpWiNs acquire enhanced responses to reward-predicting odors**
262 The UpWiN cluster collectively receives olfactory information from the MBONs and lateral
263 horn output neurons (LHONs) (Figure 3C). This anatomy raises the intriguing possibility
264 that UpWiNs have basal odor responses and memories in the MB modify it. To test this
265 possibility, we optogenetically induced appetitive memory and monitored the change in
266 the subsequent odor-evoked electrophysiological activity of UpWiNs. For these
267 experiments, we used another UpWiNs split-GAL4 driver SS67249. This driver was not
268 suitable for behavioral experiments due to stochastic and off-targeted expression but
269 labeled a highly restricted subset (1-3 cells) of UpWiNs including the one resembling the
270 morphology of SMP353 (Figure 5-figure supplement 1). Before training, the UpWiNs
271 showed relatively weak odor responses likely because inhibitory and excitatory inputs
272 cancel each other (Figure 4C). After pairing an odor with optogenetic activation of the
273 reward DANs including those projecting to α1, UpWiNs displayed increased excitatory
274 response to subsequent exposures to the CS+ odor but not to the CS- odor (Figure 5).
275 We observed the enhancement of CS+ response irrespective of the identity of tested CS+

odors (OCT or MCH; Figure 5-figure supplement 2). This enhancement of CS+ response can be most easily explained as an outcome of disinhibition from MBON-α1 whose output had been decreased by memory formation; MBON-α1 is inhibitory to UpWiNs (Figure 4B) and MBON-α1 response to the CS+ is reduced following the same training protocol (Yamada et al., n.d.).

UpWiNs promote wind-directed behaviors

Having examined the functional connectivity and plasticity of UpWiNs, we revisited behavioral phenotypes caused by optogenetic activation. In the screening experiments shown in Figure 2, since the default wind direction is from the periphery to the center in our olfactory arena, upon activation of UpWiNs**,** flies moved toward the periphery and increased their mean distance from the center. However, this phenotype might be explained by the avoidance of center area (Besson and Martin, 2005) rather than wind-directed behavior. However, several experiments argue against that possibility. First, the UpWiN activation phenotype was starvation dependent; only starved flies showed robust upwind locomotion upon UpWiN activation (Figure 6A). Second, flies' response to UpWiN activation depended on the rate and direction of the airflow. Flies did not move toward the periphery without airflow (Video 3) and moved toward the center when the direction of airflow was reversed (Figure 6B). Finally, unilateral, or bilateral ablation of aristae, the wind-sensing organ in Drosophila (Yorozu et al., 2009), impaired movement toward the periphery during UpWiN activation (Figure 6C; Video 4). These observations are consistent with a role for UpWiNs in transforming appetitive memory into wind-directed behaviors.

As observed in memory-driven olfactory responses (Figure 1 and Figure 1-figure supplement 1), the kinematics of behavior at the onset of UpWiN activation depended on

302 the initial orientation of flies relative to the wind-direction (Video 2). Flies transiently
303 increased angular speed during the first ~300ms (Figure 6D). This increased angular
304 speed was observed also in empty-split-GAL4 control flies and considered to be a startle
305 response to activating light. However, direction of turning during this period was
306 significantly biased toward the upwind direction when either of two lines for UpWiNs were
307 used to express CsChrimson (Figure 6E-F). UpWiNs activation also modulated forward
308 walking speed in a manner that depended on the orientation of flies at the onset of the
309 activating light (Figure 6G). The orientation-dependent modulation of turning direction and
310 walking speed observed is similar to that evoked by α1-specific memory (Figure 1G). In
311 contrast, activation of MBON-γ2α′1 with MB077B split-GAL4 modulated forward walking
312 speed and promoted flies that already faced upwind to maintain that orientation but did
313 not cause directional turning toward the upwind direction (Figure 6D-G; see Figure 6-figure
314 supplement 1 for other drivers). These results are consistent with a view that UpWiNs
315 transform memory in a α1 into signals that promote olfactory navigation but do not yet
316 specify lower-level motor parameters (i.e. turning direction and acceleration). Information
317 about wind-direction and UpWiN's activity needs to be integrated somewhere downstream
318 to compute the turn direction. The central complex is the likely brain area for such a
319 computation (Matheson et al., 2022; Okubo et al., 2020).
320

321 **UpWiNs are required for memory-driven upwind locomotion**

322 Finally, we asked if UpWiNs are required for retrieval of sugar-induced appetitive memory.
323 Formation of long-lasting appetitive memory after odor-sugar conditioning relies on the
324 DANs that innervate the α1 compartment (Ichinose et al., 2021; Yamagata et al., 2015).
325 Therefore, we tested the requirement of UpWiNs for 1-day appetitive memory. The control
326 genotypes showed enhanced upwind locomotion in the presence of odors associated with
327 sugar, whereas flies that express the light chain of tetanus toxin (TNT) in UpWiNs showed

328 compromised upwind-locomotion (Figure 7A-B). To test the requirement of UpWiNs
329 specifically during the memory test period, we also attempted experiments with
330 temperature-sensitive *shibire*, which allows reversible block of vesicular release
331 (Kitamoto, 2001). One day after odor-sugar conditioning, blocking synaptic output of
332 UpWiNs only during test period impaired preference to CS+ odor in binary choice
333 compared to the genetic controls (Figure 7C). However, we were unable to analyze wind-
334 directional behaviors in these *shibire* experiments because control flies did not show CS+
335 odor-induced upwind locomotion at restrictive temperature (data not shown) presumably
336 due to increased preference to the peripheral of the arena or altered odor concentration.
337 These results indicate that UpWiNs play a major role in behavior during appetitive memory
338 retrieval but also suggest that their behavioral contribution may not be limited to simple
339 promotion of upwind locomotion. Indeed, the analysis of 10s activation screening data
340 revealed that flies increased the probability of revisiting the location where UpWiNs were
341 activated (Figure 2B), although this data doesn't necessarily indicate induction of spatial
342 memory by UpWiNs and we found that another cell types SMP357-362 defined by
343 SS49755-split-GAL4 caused far more robust revisiting phenotype (Figure 2B; Video 5).
344 Also, optogenetic activation of the UpWiNs could bias spatial distribution of flies between
345 quadrants with and without activating illumination (Figure 7D). This bias is likely due to the
346 airflow-independent function of UpWiNs because the UpWiN activation could increase the
347 probability of revisiting behavior even in the absence of airflow (Figure 7E and Figure 7-
348 figure supplement 1).
349

350 **Discussion**

351 It has been postulated that the valence of learned odors is represented as the relative
352 activity of the MBONs, each of which signals either positive or negative valence assigned
353 in the parallel memory modules. In this study, we identified a cluster of neurons that can

354 decode the differential activity of MBONs encoding opposing valances. Although activity
355 of these neurons strongly induced a coordinated sequence of motor patterns that are
356 deeply related to olfactory navigation, determination of turning direction and walking speed
357 depended on fly's orientation to wind direction. Thus, our findings may mark an important
358 transition point of the circuit, where abstract valence signals encoded by a population of
359 neurons are evaluated and gradually transformed into concrete motor patterns.
360

361 **Memory valence and competing drives**

362 Previous studies in the Drosophila MB have predicted the existence of a valence integration
363 process. First, flies can create appetitive and aversive memories in parallel in different MB
364 compartments after a single learning experience, and those memories compete over the
365 behavioral choice with distinct time courses (Aso et al., 2014b; Aso and Rubin, 2016; Das et
366 al., 2014; Kaun et al., 2011). Second, memory extinction (Felsenberg et al., 2018) and
367 reversal learning (McCurdy et al., 2021) create a memory trace in a MB compartment, which
368 neutralizes the effect of the original memory traces that persist in other MB compartments.
369 Third, attraction and avoidance behaviors induced by photoactivation of multiple types of
370 MBONs can be largely explained by the additive effects of individual activation (Aso et al.,
371 2014b).
372

373 These studies support the "valence-balance model", where learning-induced plasticity in the
374 MB tips the balance of the valence signals of the MBON population (Heisenberg, 2003; Hige,
375 2018; Modi et al., 2020; Owald and Waddell, 2015). The mode of synaptic integration
376 observed in the UpWiNs matches the expectation from this model. UpWiNs receive direct
377 inhibitory and excitatory synaptic inputs from MBONs of appetitive and aversive memory

compartments, respectively. When both presynaptic MBONs were activated, which mimicked the naive state (i.e. no depression in either of the MBONs), those inputs canceled each other, resulting in no net excitation (Figure 4). When plasticity was induced in the inhibitory appetitive-memory MBONs, which mimics appetitive memory formation, the odor response was enhanced (Figure 5). Thus, UpWiNs are able to decode the unbalanced activity of MBONs encoding opposing valence. Given the prevalence of convergent circuit motifs in the downstream circuits of the MB (Li et al., 2020), we predict that similar synaptic integration of those output neurons that signal the same or opposite stimulus valences controls other components of olfactory behaviors. Convergence of valence signals might also occur between the MB and LH, which is the other olfactory center parallel to the MB and is thought to mediate innate behavior. In fact, one MBON type sends its axon to the LH and causes learning-dependent modulation of the activity of food-odor-responding neurons (Dolan et al., 2018). UpWiNs also receive abundant input from the LH neurons, suggesting that UpWiNs also play an important role in integrating the innate and learned valances. The use of divergent and convergent pathways to process valence signals, like those we describe here, appear to be an evolutionarily conserved strategy that is observed, for example, in the vertebrate amygdala and its associated brain areas (Tye, 2018).

UpWiNs and olfactory navigation

In addition to valence integration, UpWiNs play an important role in wind-guided behavior. Wind direction provides a critical cue for olfactory navigation in natural environments where odorants are propagated by the stream of airflow. Male moths have an astonishing ability to track the source of attractant pheromones emitted from females located over a mile away, and have been used as a model for olfactory navigation (Cardé, 2021; Kanzaki and Ikeda,

402 1994; Vergassola et al., 2007). Male moths react to the intermittent plume of pheromone by
403 series of cast-surge-cast actions (Baker, 1990). In a wind tunnel experiment, *Cadra cautella*
404 moths began cross-wind casting following withdrawal of the pheromone plume. Upon contact
405 with a single puff of pheromone, moths surged upwind after a delay of approximately 200 ms
406 to re-orient themselves. In our optogenetic experiments, activation of UpWiNs increased
407 angular velocity with a similar time scale and biased turning direction toward the upwind
408 direction (Figure 6D-F). In addition to promoting an upwind surge, UpWiNs activation
409 increased the probability of returning to the location where activation was applied even after
410 the cessation of both optogenetic activation and airflow (Figure 7 and Figure 7-figure
411 supplement 1). Therefore, UpWiNs alone may be able to promote a series of cast-surge-cast
412 reactions when flies navigate intermittent plumes of reward-predicting odors. Furthermore,
413 as the third function, UpWiNs relay information about reward-predicting odor to the
414 downstream neuron SMP108, which in turn feeds excitatory inputs to multiple DANs to
415 instruct formation of second-order memories (Yamada et al., n.d.). Interestingly, the patterns
416 of DAN population responses to SMP108 or UpWiNs activation are similar to those observed
417 when flies are walking toward vinegar in a virtual environment (Zolin et al., 2021). Together
418 with the evidence of inputs from the lateral horn neurons, this may indicate that UpWiNs is
419 also responsible for upwind locomotion to innately attractive odors and can be the causal
420 source of action correlates in DANs. All three of these UpWiNs functions likely contribute to
421 olfactory navigation in complex environments. Our study was limited to walking behaviors,
422 and the role of UpWiNs in flight behaviors remains to be investigated. UpWiNs are also well-
423 positioned to influence internal state to promote selective processing of wind and olfactory
424 stimuli.

425 Recent studies in Drosophila have provided insights into detailed neural circuit
426 mechanisms of wind sensation and olfactory navigation. Both flying and walking flies
427 turn upwind and increase locomotion speed when they encounter an attractive odor
428 (Álvarez-Salvado et al., 2018; Steck et al., 2012; van Breugel and Dickinson, 2014).
429 Airflow is detected by displacement of aristae and the Johnston organ sensory neurons
430 (Kamikouchi et al., 2006; Yorozu et al., 2009), and left-right asymmetry is computed by
431 the downstream neurons to represent wind direction in the central complex (Matheson et
432 al., 2022; Okubo et al., 2020; Suver et al., 2019). Fictive appetitive and aversive training
433 using optogenetic activation of DANs can promote and suppress the upwind locomotion,
434 respectively (Handler et al., 2019), suggesting that retrieval of associative memory to
435 drive behavior utilizes this same navigational strategy. Activation of a set of input
436 neurons of the fan-shaped body (FB), which is a part of the central complex known as
437 the navigation center of insects, can induce robust upwind locomotion (Matheson et al.,
438 2022). The FB is one of the major downstream targets of MBONs (Li et al., 2020;
439 Scaplen et al., 2021), while also receiving input from neurons representing wind
440 directions (Matheson et al., 2022). Although these studies point to the importance of the
441 central complex as the integration site of information about learned odor and wind
442 direction, much remains to be learned about how the valence signals conveyed by
443 MBONs influence upwind locomotion.
444 Based on the EM connectome data, SMP108 appears to be the most prominent
445 neuron postsynaptic to UpWiNs. Activation of SMP108 was able to promote upwind
446 locomotion, but the behavioral components differed from UpWiNs activation (Figure 2),
447 and blocking SMP108 did not affect retrieval of appetitive memory (Yamada et al., n.d.).
448 Therefore, UpWiNs may evoke upwind behavior through other downstream cells. FB6D,
449 FB6I and FB6T appear to be other major downstream neurons of UpWiNs (Figure 3C).
450 The top 3 downstream neurons of FB6D are hDeltaF, hDeltaC and hDeltaK. hDeltaC is

451 the columnar cell type of the FB that is known to integrate wind-directional cues and
452 information of innately attractive odor to promote upwind behavior (Matheson et al., 2022).
453 Our screening also identified that co-activation of hDeltaB, hDeltaD and hDeltaE can
454 promote robust upwind locomotion (Figure 2 and Figure 2-figure supplement 1). Thus
455 these hDelta cell types likely function together to regulate wind-directed locomotion. EM-
456 connectome-guided follow-up studies on other cell types with significant upwind/downwind
457 phenotypes (Figure 2) will help generate a comprehensive understanding of olfactory
458 navigation circuits.
459

460 **Compartment-specific contribution to anemotaxis**

461 One highlight of our study is the finding that memories stored in different MB compartments
462 use different behavioral strategies during retrieval. Although gaining a full description of
463 those behavioral strategies is beyond the scope of the present study, we can speculate on
464 the potential biological significance of the differential contributions to anemotaxis—
465 movement in response to air currents—behaviors by MB compartments.

466 First, the difference in the type of memory stored in different compartments is likely
467 to be a key factor. Based on the circuit connectivity and behavioral data, UpWiNs are
468 responsible for upwind locomotion driven by the memory stored in the α1 compartment.
469 Compared to other DANs for appetitive memory, the DANs in the α1 only weakly respond
470 to sugar (Yamagata et al., 2015), and write a memory slowly even when optogenetically
471 activated (Aso and Rubin, 2016; Yamada et al., n.d.). Once formed with repetitive training,
472 the memory in the α1 lasts over a day and is most resistant to extinction (Aso and Rubin,
473 2016; Huetteroth et al., 2015; Ichinose et al., 2015; Yamada et al., n.d.; Yamagata et al.,

474 2015). These features collectively indicate that flies undergo wind-guided olfactory
475 navigation only when they expect a robust reward associated with the odor.

476 Second, the MB must operate with different downstream circuits in adults and larva.
477 Holometabolan insects undergo complete metamorphosis by which body structures of
478 larvae abruptly develop into adult's form through pupal stage. In Drosophila, behavioral
479 components of olfactory navigation and relevant neural circuits also undergo striking
480 changes through metamorphosis. Drosophila larvae hatch from eggs with already
481 developed circuits of olfaction and an MB that consists of ~70 mature KCs, 7 DANs and 24
482 MBONs (Eichler et al., 2017). The first instar larval MB circuit is numerically simpler than
483 that of the adult but can support associative learning (Pauls et al., 2010). Larval drosophila
484 perform innate and memory-based olfactory navigation by modulating rate of head casting
485 and reorientation based on concentration gradient of odors measured over time (Fishilevich
486 et al., 2005; Saumweber et al., 2018). Although larvae can sense wind and use it to avoid
487 aversive odors (Jovanic et al., 2019), they do not use the wind direction to localize the source
488 of attractive odors as adults do. The adult airflow-sensing organ (i.e., aristae), relevant
489 neural circuits such as the central complex, legs and wings all develop during
490 metamorphosis. Therefore, the metamorphing MB circuit must adopt new interacting
491 partners to transform stored memories into adult-specific anemotaxis behaviors.

492 The EM connectome of larval and adult MB circuits revealed many cell types with
493 similar morphology, which are in some cases labeled by the same genetic driver lines (Aso
494 et al., 2014a; Eichler et al., 2017; Li et al., 2020). To unambiguously match larval and adult
495 cell types, a recent study followed full developmental trajectories of larval MB cell types into
496 the adult MB by immobilizing expression patterns of genetic driver lines (Truman et al.,
497 2022). Intriguingly, a large fraction of MBONs and DANs survive through metamorphosis

498 and become a part of the adult MB circuit. For instance, among 17 types of larval MBONs
499 examined, 10 types developed into adult MBONs. These larval-origin MBONs arborize their
500 dendrites in the γ or β′ lobes. Our experiments indicated that appetitive memories in γ4 and
501 γ5β′2a compartments can bias the choice between quadrants filled with CS+ and CS- odors
502 but do not promote walking toward upwind (Figure 1). This could be because the γ lobe
503 stores both olfactory and visual memories (Vogt et al., 2016, 2014); walking upwind does
504 not help get closer to visual cues associated with reward. On the other hand, α/β KCs,
505 MBON-α1, MBON-α3, MBON-β1>α are adult specific cell types. Notably, MBON-β1>α
506 innervates the α lobe and is directly connected with MBON-α1 and MBON-α3, suggesting
507 that UpWiNs may integrate information from the β1, α1 and α3. These anatomical
508 observations suggest that the adult-specific output pathways of MB may be dedicated to
509 anemotaxis. In naturalistic olfactory conditioning with sugar reward, flies form parallel
510 appetitive memories in compartments of both larval-origin and adult-specific MBONs. Future
511 EM-connectome-guided studies will elucidate how the adult MB integrates parallel
512 memories to synthesize navigational strategies by blending anemotactic and other
513 behavioral components.
514

515 **Acknowledgments**

516 We thank Gerald M. Rubin, Glenn Turner, Ashok Litwin-Kumar, Daisuke Hattori, Gown
517 Turvo, Huai-ti Lin and members of the Y.A. and T.H. labs for valuable discussion and
518 comments on the manuscript. We thank Feng Li, Marisa Dreher, Christina Christoforou,
519 Kari Close and the members of Janelia FlyEM, Flylight, fly facility, Project Technical
520 Resource and scientific computing for technical support. D.Y. was supported by Toyobo
521 Biotechnology Foundation Postdoctoral Fellowship and Japan Society for the Promotion

522 of Science Overseas Research Fellowship. Y.A. was supported by HHMI. T.H. was
523 supported by NIH (R01DC018874), NSF (2034783), BSF (2019026) and UNC Junior
524 Faculty Development Award.

525 **Declaration of interests**

526 The authors declare no competing interests.

527 **CONTACT FOR REAGENT AND RESOURCE SHARING**
528 Further information and requests for resources and reagents should be directed to and will
529 be fulfilled by Yoshinori Aso (asoy@janelia.hhmi.org) or Toshihide Hige
530 (hige@email.unc.edu)

531 **METHOD DETAILS**

532 **Fly strains**
533 *Drosophila melanogaster* strains were reared at 22C and 60% humidity on standard
534 cornmeal food in a 12:12 hour light:dark cycle. 4-10-day-old adult females were used 2-4
535 days after sorting them on a Peltier cold plate. For flies expressing CsChrimson (Klapoetke
536 et al., 2014) the food was supplemented with retinal (0.2 mM all-trans-retinal prior to eclosion
537 and then 0.4 mM). Driver and effector lines are listed in KEY RESOURCE TABLE and
538 genotypes used by each figure are listed below. The new collection of split-GAL4 drivers was
539 designed based on confocal image databases (http://flweb.janelia.org)(Jenett et al., 2012),
540 and screening expression patterns of p65ADZp and ZpGAL4DBD combinations as described
541 previously (Aso et al., 2014a; Pfeiffer et al., 2010). Confocal stacks of new split-GAL4 driver
542 lines used in this study are available at http://www.janelia.org/split-gal4.

543 **Olfactory conditioning**

544 Olfactory conditioning was performed as previously described (Aso and Rubin, 2016).
545 Groups of approximately 20 females of 4–10 d post-eclosion were trained and tested using
546 the modified four-field olfactory arena (Aso and Rubin, 2016; Pettersson, 1970) equipped
547 with a 627nm LED board (34.9 μW/mm2 at the position of the flies) and odor mixers. The
548 flow rate of input air from each of the four arms was maintained at 100 mL/min throughout
549 the experiments by mass-flow controllers, and air was pulled from the central hole at
550 400 mL/min. Odors were delivered to the arena by switching the direction of airflow to the
551 tubes containing diluted odors using solenoid valves. The odors were diluted in paraffin
552 oil: pentyl acetate (PA: 1:10000) and ethyl lactate (EL: 1:10000). Sugar conditioning was
553 performed by using tubes with sucrose absorbed Whatman 3 MM paper that was dried
554 before use as previously described (Krashes and Waddell, 2008; Liu et al., 2012). For
555 conditioning with optogenetic activation of DANs, 60 s of odor was paired with 30 times 1
556 s of red LED light with 1s gaps. LED pulses started 5 s after the opening of odor valves.
557 Before conditioning, flies were starved for 40-48 hour on 1% agar. Videography was

performed at 30 frames per second and analyzed using Flytracker (https://github.com/kristinbranson/FlyTracker) or Fiji. For experiments using one day memory retention, flies were kept in agar vials at 21C after first-order conditioning. For testing olfactory memories, the distribution of flies in the four quadrants was measured for 60 s. The performance index (PI) is defined as a mean of [(number of flies in the two diagonal quadrants filled with odor one) - (number of flies in other two quadrants filled with odor two or air)]/(total number of flies) during the final 30 s of the 60 s test period. The average PI of reciprocal experiments is shown in figures to cancel out potential position bias and innate odor preference.

Airflow response

For testing airflow directional response, each fly's distance from center (r_i) was measured. The radius of the arena, r_{arena}, was 50 mm. Because of the circular shape of the arena, the area of particular r bin is larger as r increases. For instance, the area of 40<r<50mm is 9 times larger than the area of 0<r<10 mm. When flies distribute randomly in the arena, the mean r_i is 1/sqrt(2). To normalize this area difference we used the square of (r_i/r_{arena}) as an area-normalized distance from the center index. To calculate upwind displacement, the mean of area-normalized distance from center at each time point in each movie was subtracted by the area-normalized distance at the onset of activating illumination or odor presentation. To compensate for the delay between the switch of solenoid valves and delivery of the odor (~2 s) as well as the time to fill the arena with odorized air (~3 s), the onset of odor was taken to be 3.5 seconds after the switch of solenoid valves. For analysis of individual trajectories, only flies that were more than 3 mm away from the edge of the arena were analyzed. Trajectories with too abrupt changes of angle (more than 180 degree) or position (more than 5mm) in one frame were considered as tracking errors and excluded from the analysis. The direction toward the center of the arena, where suction tubing is connected, was designed as +/-180 degrees relative to the upwind direction. For analyzing the influence of initial orientation on directional turning and forward walking speed, subsets of trajectories were analyzed by grouping them into +/- 30 degree bins of initial angle.

Electrophysiology

Electrophysiological experiments were performed as previously described (Yamada et al., n.d.). Briefly, flies were collected on the day of eclosion and kept in the dark on all-trans-retinal food (0.5 mM) until experiments for 48-72 hr. The patch pipettes (6-7 MΩ) were filled with the pipette solution containing (in mM): L-potassium aspartate, 140; HEPES, 10; EGTA, 1.1; $CaCl_2$, 0.1; Mg-ATP, 4; Na-GTP, 0.5 with pH adjusted to 7.3 with KOH (265 mOsm). The preparation was continuously perfused with saline containing (in mM): NaCl, 103; KCl, 3; $CaCl_2$, 1.5; $MgCl_2$, 4; $NaHCO_3$, 26; N-tris(hydroxymethyl) methyl-2-aminoethane-sulfonic acid, 5; NaH_2PO_4, 1; trehalose, 10; glucose, 10 (pH 7.3 when bubbled with 95% O_2 and 5% CO_2, 275 mOsm). UpWiNs were visually identified by fluorescence signals expressed by specific drivers. Whole-cell recordings were made using the Axon MultiClamp 700B amplifier (Molecular Devices). Cells were held at around -60 mV by injecting hyperpolarizing current, which was typically less than 10 pA. Signals were low-pass filtered at 5 kHz and digitized at 10 kHz before being acquired and analyzed by custom MATLAB scripts (MathWorks). Subthreshold odor responses were quantified by averaging the mean depolarization above the baseline during 0 to 1.2 s after odor onset. Saturated head-space vapors of odors were presented to flies after 1 % air dilution using a custom odor delivery system. 625 nm LEDs were used to deliver photostimulation at 17 mW/mm^2 through the objective lens.

606

607 **Calcium imaging**

608 All experiments were performed on female flies, 3-7 days after eclosion. Brains were
609 dissected in a saline bath (103 mM NaCl, 3 mM KCl, 2 mM CaCl2, 4 mM MgCl2, 26 mM
610 NaHCO3, 1 mM NaH2PO4, 8 mM trehalose, 10 mM glucose, 5 mM TES, bubbled with 95%
611 O2 / 5% CO2). After dissection, the brain was positioned anterior side up on a coverslip in
612 a Sylgard dish submerged in 3 ml saline at 20℃. The sample was imaged with a resonant
613 scanning 2-photon microscope with near-infrared excitation (920 nm, Spectra-Physics,
614 INSIGHT DS DUAL) and a 25X objective (Nikon MRD77225 25XW). The microscope was
615 controlled using ScanImage 2016 (Vidrio Technologies). Images were acquired over a 231
616 µm × 231 µm x 42 µm volume with a step size at 2 µm. The field of view included 512 × 512
617 pixel resolution taken at approximately 1.07 Hz frame rate. The excitation power during
618 imaging was 19 mW.

619 For photostimulation, the light-gated ion channel Chrimson88 was activated with a 660-
620 nm LED (M660L3 Thorlabs) coupled to a digital micromirror device (Texas Instruments
621 DLPC300 Light Crafter) and combined with the imaging path using a FF757-DiO1 dichroic
622 (Semrock). On the emission side, the primary dichroic was Di02-R635 (Semrock), the
623 detection arm dichroic was 565DCXR (Chroma), and the emission filters were FF03-525/50
624 and FF01-625/90 (Semrock). Photostimulation occurred over a 1 s period at a 12 µW/mm2
625 intensity over 9 consecutive trials interspersed by a 30 s period. The light intensity was
626 measured using a Thorlabs S170C power sensor.

627 When quantifying the GCaMP fluorescence, ROIs corresponding to mushroom body
628 compartments were drawn using custom python scripts on images showing the maximum
629 intensity over time. Mean intensity changes within these ROIs were measured in the time
630 series images. Final intensity measurements subtracted a background ROI that was drawn
631 in a region with no fluorescence. Baseline fluorescence is the mean fluorescence over a 5 s
632 time period before stimulation started. The ΔF was then divided by baseline to normalize the
633 signal (ΔF/F). The mean responses from the 9 trials were calculated for each animal (5-11
634 samples per driver).

635

636 **Analysis of connectivity and morphology**

637 The information was retrieved from neuPrint (neuprint.janelia.org) hosting the "hemibrain"
638 dataset (Scheffer et al., 2020), which is a publicly accessible web site
639 (https://doi.org/10.25378/janelia.12818645.v1). For cell types, we cited cell type assignments
640 reported in Scheffer et al., 2020. Only connections of the cells in the right hemisphere were
641 used due to incomplete connectivity in the left hemisphere (Zheng et al., 2018). Connectivity
642 data was then imported into Cytoscape (https://cytoscape.org/) for generating circuit
643 diagrams that were edited using Adobe Illustrator. The 3D renderings of neurons presented
644 were generated using the visualization tools of NeuTu (Zhao et al., 2018) or VVD viewer
645 (https://github.com/takashi310/VVD_Viewer;(Wan et al., 2012). Morphological similarity of
646 individual neurons in SS33917 driver was performed by NBLAST (Costa et al., 2016).

647

648 **Immunohistochemistry**

649 Brains and ventral nerve cord of 4-10 days old females were dissected, fixed and
650 immunolabeled as previously described using the antibodies listed in Key Resource
651 Table(Aso et al., 2014a; Nern et al., 2015).

652

653 **Statistics**

654 Statistical comparisons were performed on Graphpad Prism or MATLAB using the Kruskal
655 Wallis test followed by Dunn's post-test for multiple comparison, t-te tests, or two-way

656 ANOVA followed by Tukey's post hoc multiple comparisons test as designated in figure
657 legends.
658
659
660 **Detailed fly genotypes used by figures**

Figure	Genotype
Figure 1D-H Figure 1-Figure supplement 1	*w/w, 20xUAS-CsChrimson-mVenus attP18;;+/MB043C-split-GAL4* *w/w, 20xUAS-CsChrimson-mVenus attP18;+/MB213B-split-GAL4* *w/w, 20xUAS-CsChrimson-mVenus attP18;;+/MB312C-split-GAL4* *w/w, 20xUAS-CsChrimson-mVenus attP18;MB109B/MB315C-split-GAL4* *w/w, 20xUAS-CsChrimson-mVenus attP18;+/ Empty-split-GAL4*
Figure 2 Figure 2 -figure supplement 1 and 2	*w/w, 20xUAS-CsChrimson-mVenus attP18;Split-GAL4/+*
Figure 3A	*w/w, 20xUAS-CsChrimson-mVenus attP18;SS33917-Split-GAL4/+*
Figure 3 - figure supplement 2	*pBPhsFlp2::PEST in attP3;; pJFRC201-10XUAS-FRT>STOP>FRT-myr::smGFP-HA in VK0005, pJFRC240-10XUAS- FRT>STOP>FRT-myr::smGFP-V5-THS-10XUAS-FRT>STOP>FRT-myr::smGFP-FLAG in su(Hw)attP1/SS33917-split-GAL4*
Figure 4A Figure 4B Figure 4C	*LexAop2-Syn21-opGCaMP6s (JK16F), LexAop2-Syn21-opGCaMP6s (SuHwattP8), 10XUAS-Syn21-Chrimson88-tdT-3.1 (attP18)/+; R64A11-LexAp65 (JK73A)/MB082C* *LexAop2-Syn21-opGCaMP6s (JK16F), LexAop2-Syn21-opGCaMP6s (SuHwattP8), 10XUAS-Syn21-Chrimson88-tdT-3.1 (attP18)/+; R64A11-LexAp65 (JK73A)/MB310C* *LexAop2-Syn21-opGCaMP6s (JK16F), LexAop2-Syn21-opGCaMP6s (SuHwattp8), 10xUAS-Syn21-Chrimson88-tdT-3.1 (attp18); G0239-GAL4/G0239-GAL4; R64A11-LexAp65 (JK73A)/+* *LexAop2-Syn21-opGCaMP6s (JK16F), LexAop2-Syn21-opGCaMP6s (SuHwattp8), 10xUAS-Syn21-Chrimson88-tdT-3.1 (attp18); G0239-GAL4/G0239-GAL4; R64A11-LexAp65 (JK73A)/MB310C* *LexAop2-Syn21-opGCaMP6s (JK16F), LexAop2-Syn21-opGCaMP6s (SuHwattp8), 10xUAS-Syn21-Chrimson88-tdT-3.1 (attp18); G0239-GAL4/+; R64A11-LexAp65 (JK73A)/MB310C*
Figure 5	*13XLexAop2-IVS-p10-ChrimsonR-mVenus (attP18); 58E02-LexAp65 (attP40)/ss67249-split1; pJFRC28-10XUAS-IVS-GFP-p10 (SuHwattP1) / ss67249-split2*
Figure 5 -figure supplement 1	*pBPhsFlp2::PEST in attP3;; pJFRC201-10XUAS-FRT>STOP>FRT-myr::smGFP-HA in VK0005, pJFRC240-10XUAS- FRT>STOP>FRT-myr::smGFP-V5-THS-10XUAS-FRT>STOP>FRT-myr::smGFP-FLAG in su(Hw)attP1/SS67249-split-GAL4*
Figure 5 -figure supplement 2	*13XLexAop2-IVS-p10-ChrimsonR-mVenus (attP18); 58E02-LexAp65 (attP40)/ss67249-split1; pJFRC28-10XUAS-IVS-GFP-p10 (SuHwattP1) / ss67249-split2*
Figure 6	*w/w, 20xUAS-CsChrimson-mVenus attP18;SS33917-Split-GAL4/+* *w/w, 20xUAS-CsChrimson-mVenus attP18;SS33918-Split-GAL4/+* *w/w, 20xUAS-CsChrimson-mVenus attP18;MB077B-Split-GAL4/+* *w/w, 20xUAS-CsChrimson-mVenus attP18;Empty-Split-GAL4/+*
Figure 6 -figure supplement 1	*w/w, 20xUAS-CsChrimson-mVenus attP18;Split-GAL4/+*

Figure 7A-B	*w/+;SS33917-split-GAL4/+* *w/+; SS33917-split-GAL4UAS-TNT (II)* *w/+; Empty-split-GAL4UAS-TNT (II)*
Figure 7C	*w/w;VT007746-p65ADZp in attP40/20xUAS-Shbire-p10 in VK00005* *w/w;R64A11-ZpGAL4DBD in attP2/20xUAS-Shbire-p10 in VK00005* *w/w;SS33917(VT007746-p65ADZp in attP40; R64A11-ZpGAL4DBD in attP2)/20xUAS-Shbire-p10 in VK00005* *w/w;Empty-split-GAL4/20xUAS-Shbire-p10 in VK00005*
Figure 7D	*w/w, 20xUAS-CsChrimson-mVenus attP18;SS33917/+* *w/w, 20xUAS-CsChrimson-mVenus attP18;Empty-split-GAL4 /+*
Figure 7E	*w/w, 20xUAS-CsChrimson-mVenus attP18;SS33917/+* *w/w, 20xUAS-CsChrimson-mVenus attP18;SS33918/+* *w/w, 20xUAS-CsChrimson-mVenus attP18;SS49755/+* *w/w, 20xUAS-CsChrimson-mVenus attP18;Empty-split-GAL4 /+*
Figure 7 -figure supplement 1	*w/w, 20xUAS-CsChrimson-mVenus attP18;SS33917/+* *w/w, 20xUAS-CsChrimson-mVenus attP18;SS33918/+* *w/w, 20xUAS-CsChrimson-mVenus attP18;SS49755/+* *w/w, 20xUAS-CsChrimson-mVenus attP18;Gr64f-GAL4;Gr64f-GAL4/+* *w/w, 20xUAS-CsChrimson-mVenus attP18;Empty-split-GAL4 /+*

Data and Code Availability

The confocal images of expression patterns are available online (http://www.janelia.org/split-gal4). The values used for figures are summarized in Supplementary File 2. The design files of the olfactory arena are available at flintbox (https://hhmi.flintbox.com/technologies/c65b2ddd-3cc1-44d9-a95d-73e08723f724).

Supplemental information

Video 1. Activation phenotype of UpWiNs
An example movie of UpWiN activation in SS33917>CsChrimson flies used in Figure 2. The red square at the bottom right corner indicates the 10s period when the red LED was turned on. The small circles indicate the centroid of flies and triangles indicate the orientation of flies.

Video 2. Activation phenotype of UpWiNs depends on the initial orientation
Cropped movies of individual SS33917>CsChrimson flies centered and reoriented based on the position and the angle to upwind at the onset of the activating illumination (related to Figure 2 and Figure 6D-G). The red square at the bottom right corner of each panel indicates when the red LED was turned on. The small circles indicate the centroid of flies and triangles indicate the orientation of flies. The airflow direction was from the top to the bottom of each panel.

Video 3. Activation phenotype of UpWiNs without airflow
An example movie of UpWiN activation in SS33917>CsChrimson flies without airflow (related to Figure 6B).

Video 4. Activation phenotype of UpWiNs depends on the intact aristae

An example UpWiN activation phenotype in an SS33917>CsChrimson fly that lacked the arista on the right side (related to Figure 6C).

Video 5. Return phenotype induced by SMP357-362 activation

An example movie of SMP357-362 activation in SS49755>CsChrimson flies. The red square at the bottom right corner indicates the 10s period when the red LED was turned on. The small circles indicate the centroid of flies and triangles indicate the orientation of flies. Trajectories of flies after turning off LED are shown as lines connecting centroids over time.

Supplementary File 1: **KEY RESOURCES TABLE**

Supplementary File 2: **Data TABLE**

References

Álvarez-Salvado E, Licata AM, Connor EG, McHugh MK, King BMN, Stavropoulos N, Victor JD, Crimaldi JP, Nagel KI. 2018. Elementary sensory-motor transformations underlying olfactory navigation in walking fruit-flies. *Elife* **7**:e37815.

Aso Y, Hattori D, Yu Y, Johnston RM, Iyer NA, Ngo T-TB, Dionne H, Abbott LF, Axel R, Tanimoto H, Rubin GM. 2014a. The neuronal architecture of the mushroom body provides a logic for associative learning. *Elife* **3**:e04577.

Aso Y, Rubin GM. 2016. Dopaminergic neurons write and update memories with cell-type-specific rules. *Elife* **5**. doi:10.7554/eLife.16135

Aso Y, Sitaraman D, Ichinose T, Kaun KR, Vogt K, Belliart-Guérin G, Plaçais P-Y, Robie AA, Yamagata N, Schnaitmann C, Rowell WJ, Johnston RM, Ngo T-TB, Chen N, Korff W, Nitabach MN, Heberlein U, Preat T, Branson KM, Tanimoto H, Rubin GM. 2014b. Mushroom body output neurons encode valence and guide memory-based action selection in Drosophila. *Elife* **3**:e04580.

Baker TC. 1990. Upwind flight and casting flight : Complementary phasic and tonic systems used for location of sex pheromone sources by male moth. *Proc 10th Int Symp Olfaction and Taste, Oslo* **18-25**.

Berry JA, Phan A, Davis RL. 2018. Dopamine Neurons Mediate Learning and Forgetting through Bidirectional Modulation of a Memory Trace. *Cell Rep* **25**:651–662.e5.

Besson M, Martin J-R. 2005. Centrophobism/thigmotaxis, a new role for the mushroom bodies in Drosophila. *J Neurobiol* **62**:386–396.

Beyeler A, Namburi P, Glober GF, Simonnet C, Calhoon GG, Conyers GF, Luck R, Wildes CP, Tye KM. 2016. Divergent Routing of Positive and Negative Information from the Amygdala during Memory Retrieval. *Neuron* **90**:348–361.

Bogovic JA, Otsuna H, Heinrich L, Ito M, Jeter J, Meissner G, Nern A, Colonell J, Malkesman O, Ito K, Saalfeld S. 2020. An unbiased template of the Drosophila brain and ventral nerve cord. *PLoS One* **15**:e0236495.

Campbell RAA, Honegger KS, Qin H, Li W, Demir E, Turner GC. 2013. Imaging a population code for odor identity in the Drosophila mushroom body. *J Neurosci* **33**:10568–10581.

Cardé RT. 2021. Navigation Along Windborne Plumes of Pheromone and Resource-

739 Linked Odors. *Annu Rev Entomol* **66**:317–336.
740 Cohn R, Morantte I, Ruta V. 2015. Coordinated and Compartmentalized
741 Neuromodulation Shapes Sensory Processing in Drosophila. *Cell* **163**:1742–1755.
742 Costa M, Manton JD, Ostrovsky AD, Prohaska S, Jefferis GSXE. 2016. NBLAST: Rapid,
743 Sensitive Comparison of Neuronal Structure and Construction of Neuron Family
744 Databases. *Neuron* **91**:293–311.
745 Das G, Klappenbach M, Vrontou E, Perisse E, Clark CM, Burke CJ, Waddell S. 2014.
746 Drosophila learn opposing components of a compound food stimulus. *Curr Biol*
747 **24**:1723–1730.
748 Dolan M-J, Belliart-Guérin G, Bates AS, Frechter S, Lampin-Saint-Amaux A, Aso Y,
749 Roberts RJV, Schlegel P, Wong A, Hammad A, Bock D, Rubin GM, Preat T, Plaçais
750 P-Y, Jefferis GSXE. 2018. Communication from Learned to Innate Olfactory
751 Processing Centers Is Required for Memory Retrieval in Drosophila. *Neuron*
752 **100**:651–668.e8.
753 Eckstein N, Bates AS, Du M, Hartenstein V, Jefferis GSX, Funke J. n.d.
754 Neurotransmitter Classification from Electron Microscopy Images at Synaptic Sites
755 in Drosophila. doi:10.1101/2020.06.12.148775
756 Eichler K, Li F, Litwin-Kumar A, Park Y, Andrade I, Schneider-Mizell CM, Saumweber T,
757 Huser A, Eschbach C, Gerber B, Fetter RD, Truman JW, Priebe CE, Abbott LF,
758 Thum AS, Zlatic M, Cardona A. 2017. The complete connectome of a learning and
759 memory centre in an insect brain. *Nature*. doi:10.1038/nature23455
760 Felsenberg J, Jacob PF, Walker T, Barnstedt O, Edmondson-Stait AJ, Pleijzier MW, Otto
761 N, Schlegel P, Sharifi N, Perisse E, Smith CS, Lauritzen JS, Costa M, Jefferis
762 GSXE, Bock DD, Waddell S. 2018. Integration of Parallel Opposing Memories
763 Underlies Memory Extinction. *Cell* **175**:709–722.e15.
764 Fishilevich E, Domingos AI, Asahina K, Naef F, Vosshall LB, Louis M. 2005. Chemotaxis
765 behavior mediated by single larval olfactory neurons in Drosophila. *Curr Biol*
766 **15**:2086–2096.
767 Gore F, Schwartz EC, Brangers BC, Aladi S, Stujenske JM, Likhtik E, Russo MJ, Gordon
768 JA, Salzman CD, Axel R. 2015. Neural Representations of Unconditioned Stimuli in
769 Basolateral Amygdala Mediate Innate and Learned Responses. *Cell* **162**:134–145.
770 Grewe BF, Gründemann J, Kitch LJ, Lecoq JA, Parker JG, Marshall JD, Larkin MC,
771 Jercog PE, Grenier F, Li JZ, Lüthi A, Schnitzer MJ. 2017. Neural ensemble
772 dynamics underlying a long-term associative memory. *Nature* **543**:670–675.
773 Handler A, Graham TGW, Cohn R, Morantte I, Siliciano AF, Zeng J, Li Y, Ruta V. 2019.
774 Distinct Dopamine Receptor Pathways Underlie the Temporal Sensitivity of
775 Associative Learning. *Cell* **178**:60–75.e19.
776 Heisenberg M. 2003. Mushroom body memoir: from maps to models. *Nat Rev Neurosci*
777 **4**:266–275.
778 Hige T. 2018. What can tiny mushrooms in fruit flies tell us about learning and memory?
779 *Neuroscience Research*. doi:10.1016/j.neures.2017.05.002
780 Hige T, Aso Y, Modi MN, Rubin GM, Turner GC. 2015a. Heterosynaptic Plasticity
781 Underlies Aversive Olfactory Learning in Drosophila. *Neuron* **88**:985–998.
782 Hige T, Aso Y, Rubin GM, Turner GC. 2015b. Plasticity-driven individualization of
783 olfactory coding in mushroom body output neurons. *Nature* **526**:258–262.
784 Huetteroth W, Perisse E, Lin S, Klappenbach M, Burke C, Waddell S. 2015. Sweet taste
785 and nutrient value subdivide rewarding dopaminergic neurons in Drosophila. *Curr*
786 *Biol* **25**:751–758.
787 Ichinose T, Aso Y, Yamagata N, Abe A, Rubin GM, Tanimoto H. 2015. Reward signal in
788 a recurrent circuit drives appetitive long-term memory formation. *Elife* **4**:e10719.
789 Ichinose T, Kanno M, Wu H, Yamagata N, Sun H, Abe A, Tanimoto H. 2021. Mushroom

790 body output differentiates memory processes and distinct memory-guided
791 behaviors. *Curr Biol* **31**:1294–1302.e4.
792 Jacob PF, Waddell S. 2022. Spaced Training Forms Complementary Long-Term
793 Memories of Opposite Valence in Drosophila. *Neuron* **110**:2703.
794 Jenett A, Rubin GM, Ngo T-TB, Shepherd D, Murphy C, Dionne H, Pfeiffer BD,
795 Cavallaro A, Hall D, Jeter J, Iyer N, Fetter D, Hausenfluck JH, Peng H, Trautman
796 ET, Svirskas RR, Myers EW, Iwinski ZR, Aso Y, DePasquale GM, Enos A, Hulamm
797 P, Lam SCB, Li H-H, Laverty TR, Long F, Qu L, Murphy SD, Rokicki K, Safford T,
798 Shaw K, Simpson JH, Sowell A, Tae S, Yu Y, Zugates CT. 2012. A GAL4-driver line
799 resource for Drosophila neurobiology. *Cell Rep* **2**:991–1001.
800 Jovanic T, Winding M, Cardona A, Truman JW, Gershow M, Zlatic M. 2019. Neural
801 Substrates of Drosophila Larval Anemotaxis. *Curr Biol* **29**:554–566.e4.
802 Kamikouchi A, Shimada T, Ito K. 2006. Comprehensive classification of the auditory
803 sensory projections in the brain of the fruit fly Drosophila melanogaster. *J Comp*
804 *Neurol* **499**:317–356.
805 Kanzaki R, Ikeda A. 1994. Morphology and Physiology of Pheromone-Triggered Flip-
806 Flopping Descending Interneurons of the Male Silkworm Moth, Bombyx mori.
807 *Olfaction and Taste XI*. doi:10.1007/978-4-431-68355-1_348
808 Kaun KR, Azanchi R, Maung Z, Hirsh J, Heberlein U. 2011. A Drosophila model for
809 alcohol reward. *Nature Neuroscience*. doi:10.1038/nn.2805
810 Kirkhart C, Scott K. 2015. Gustatory learning and processing in the Drosophila
811 mushroom bodies. *J Neurosci* **35**:5950–5958.
812 Kitamoto T. 2001. Conditional modification of behavior in Drosophila by targeted
813 expression of a temperature-sensitive shibire allele in defined neurons. *J Neurobiol*
814 **47**:81–92.
815 Klapoetke NC, Murata Y, Kim SS, Pulver SR, Birdsey-Benson A, Cho YK, Morimoto TK,
816 Chuong AS, Carpenter EJ, Tian Z, Wang J, Xie Y, Yan Z, Zhang Y, Chow BY,
817 Surek B, Melkonian M, Jayaraman V, Constantine-Paton M, Wong GK-S, Boyden
818 ES. 2014. Independent optical excitation of distinct neural populations. *Nat Methods*
819 **11**:338–346.
820 Krashes MJ, Waddell S. 2008. Rapid consolidation to a radish and protein synthesis-
821 dependent long-term memory after single-session appetitive olfactory conditioning
822 in Drosophila. *J Neurosci* **28**:3103–3113.
823 Li F, Lindsey JW, Marin EC, Otto N, Dreher M, Dempsey G, Stark I, Bates AS, Pleijzier
824 MW, Schlegel P, Nern A, Takemura S-Y, Eckstein N, Yang T, Francis A, Braun A,
825 Parekh R, Costa M, Scheffer LK, Aso Y, Jefferis GS, Abbott LF, Litwin-Kumar A,
826 Waddell S, Rubin GM. 2020. The connectome of the adult Drosophila mushroom
827 body provides insights into function. *Elife* **9**. doi:10.7554/eLife.62576
828 Lin S, Owald D, Chandra V, Talbot C, Huetteroth W, Waddell S. 2014. Neural correlates
829 of water reward in thirsty Drosophila. *Nat Neurosci* **17**:1536–1542.
830 Liu C, Plaçais P-Y, Yamagata N, Pfeiffer BD, Aso Y, Friedrich AB, Siwanowicz I, Rubin
831 GM, Preat T, Tanimoto H. 2012. A subset of dopamine neurons signals reward for
832 odour memory in Drosophila. *Nature* **488**:512–516.
833 Matheson AMM, Lanz AJ, Medina AM, Licata AM, Currier TA, Syed MH, Nagel KI. 2022.
834 A neural circuit for wind-guided olfactory navigation. *Nat Commun* **13**:4613.
835 McCurdy LY, Sareen P, Davoudian PA, Nitabach MN. 2021. Dopaminergic mechanism
836 underlying reward-encoding of punishment omission during reversal learning in
837 Drosophila. *Nat Commun* **12**:1115.
838 Modi MN, Shuai Y, Turner GC. 2020. The Mushroom Body: From Architecture to
839 Algorithm in a Learning Circuit. *Annu Rev Neurosci* **43**:465–484.
840 Namburi P, Beyeler A, Yorozu S, Calhoon GG, Halbert SA, Wichmann R, Holden SS,

Mertens KL, Anahtar M, Felix-Ortiz AC, Wickersham IR, Gray JM, Tye KM. 2015. A circuit mechanism for differentiating positive and negative associations. *Nature* **520**:675–678.

Nern A, Pfeiffer BD, Rubin GM. 2015. Optimized tools for multicolor stochastic labeling reveal diverse stereotyped cell arrangements in the fly visual system. *Proc Natl Acad Sci U S A* **112**:E2967–76.

Nieh EH, Vander Weele CM, Matthews GA, Presbrey KN, Wichmann R, Leppla CA, Izadmehr EM, Tye KM. 2016. Inhibitory Input from the Lateral Hypothalamus to the Ventral Tegmental Area Disinhibits Dopamine Neurons and Promotes Behavioral Activation. *Neuron* **90**:1286–1298.

Okubo TS, Patella P, D'Alessandro I, Wilson RI. 2020. A Neural Network for Wind-Guided Compass Navigation. *Neuron* **107**:924–940.e18.

O'Neill P-K, Gore F, Salzman CD. 2018. Basolateral amygdala circuitry in positive and negative valence. *Curr Opin Neurobiol* **49**:175–183.

Otsuna H, Ito M, Kawase T. n.d. Color depth MIP mask search: a new tool to expedite Split-GAL4 creation. doi:10.1101/318006

Owald D, Felsenberg J, Talbot CB, Das G, Perisse E, Huetteroth W, Waddell S. 2015. Activity of defined mushroom body output neurons underlies learned olfactory behavior in Drosophila. *Neuron* **86**:417–427.

Owald D, Waddell S. 2015. Olfactory learning skews mushroom body output pathways to steer behavioral choice in Drosophila. *Curr Opin Neurobiol* **35**:178–184.

Pai T-P, Chen C-C, Lin H-H, Chin A-L, Lai JS-Y, Lee P-T, Tully T, Chiang A-S. 2013. Drosophila ORB protein in two mushroom body output neurons is necessary for long-term memory formation. *Proc Natl Acad Sci U S A* **110**:7898–7903.

Pauls D, Selcho M, Gendre N, Stocker RF, Thum AS. 2010. Drosophila larvae establish appetitive olfactory memories via mushroom body neurons of embryonic origin. *J Neurosci* **30**:10655–10666.

Pettersson J. 1970. An Aphid Sex Attractant. *Insect Systematics & Evolution*. doi:10.1163/187631270x00357

Pfeiffer BD, Ngo T-TB, Hibbard KL, Murphy C, Jenett A, Truman JW, Rubin GM. 2010. Refinement of tools for targeted gene expression in Drosophila. *Genetics* **186**:735–755.

Plaçais P-Y, Trannoy S, Friedrich AB, Tanimoto H, Preat T. 2013. Two pairs of mushroom body efferent neurons are required for appetitive long-term memory retrieval in Drosophila. *Cell Rep* **5**:769–780.

Saumweber T, Rohwedder A, Schleyer M, Eichler K, Chen Y-C, Aso Y, Cardona A, Eschbach C, Kobler O, Voigt A, Durairaja A, Mancini N, Zlatic M, Truman JW, Thum AS, Gerber B. 2018. Functional architecture of reward learning in mushroom body extrinsic neurons of larval Drosophila. *Nat Commun* **9**:1104.

Scaplen KM, Talay M, Fisher JD, Cohn R, Sorkaç A, Aso Y, Barnea G, Kaun KR. 2021. Transsynaptic mapping of mushroom body output neurons. *Elife* **10**. doi:10.7554/eLife.63379

Scheffer LK, Xu CS, Januszewski M, Lu Z, Takemura S-Y, Hayworth KJ, Huang GB, Shinomiya K, Maitlin-Shepard J, Berg S, Clements J, Hubbard PM, Katz WT, Umayam L, Zhao T, Ackerman D, Blakely T, Bogovic J, Dolafi T, Kainmueller D, Kawase T, Khairy KA, Leavitt L, Li PH, Lindsey L, Neubarth N, Olbris DJ, Otsuna H, Trautman ET, Ito M, Bates AS, Goldammer J, Wolff T, Svirskas R, Schlegel P, Neace E, Knecht CJ, Alvarado CX, Bailey DA, Ballinger S, Borycz JA, Canino BS, Cheatham N, Cook M, Dreher M, Duclos O, Eubanks B, Fairbanks K, Finley S, Forknall N, Francis A, Hopkins GP, Joyce EM, Kim S, Kirk NA, Kovalyak J, Lauchie SA, Lohff A, Maldonado C, Manley EA, McLin S, Mooney C, Ndama M, Ogundeyi

O, Okeoma N, Ordish C, Padilla N, Patrick CM, Paterson T, Phillips EE, Phillips EM, Rampally N, Ribeiro C, Robertson MK, Rymer JT, Ryan SM, Sammons M, Scott AK, Scott AL, Shinomiya A, Smith C, Smith K, Smith NL, Sobeski MA, Suleiman A, Swift J, Takemura S, Talebi I, Tarnogorska D, Tenshaw E, Tokhi T, Walsh JJ, Yang T, Horne JA, Li F, Parekh R, Rivlin PK, Jayaraman V, Costa M, Jefferis GS, Ito K, Saalfeld S, George R, Meinertzhagen IA, Rubin GM, Hess HF, Jain V, Plaza SM. 2020. A connectome and analysis of the adult central brain. *Elife* **9**. doi:10.7554/eLife.57443

Schnitzer M, Huang C, Luo J, Woo SJ, Roitman L, Li J, Pieribone V, Kannan M, Vasan G. n.d. Dopamine signals integrate innate and learnt valences to regulate memory dynamics. doi:10.21203/rs.3.rs-1915648/v1

Siju KP, Štih V, Aimon S, Gjorgjieva J, Portugues R, Grunwald Kadow IC. 2020. Valence and State-Dependent Population Coding in Dopaminergic Neurons in the Fly Mushroom Body. *Curr Biol* **30**:2104–2115.e4.

Steck K, Veit D, Grandy R, Badia SBI, Badia SBI, Mathews Z, Verschure P, Hansson BS, Knaden M. 2012. A high-throughput behavioral paradigm for Drosophila olfaction - The Flywalk. *Sci Rep* **2**:361.

Sun F, Zhou J, Dai B, Qian T, Zeng J, Li X, Zhuo Y, Zhang Y, Wang Y, Qian C, Tan K, Feng J, Dong H, Lin D, Cui G, Li Y. 2020. Next-generation GRAB sensors for monitoring dopaminergic activity in vivo. *Nat Methods* **17**:1156–1166.

Suver MP, Matheson AMM, Sarkar S, Damiata M, Schoppik D, Nagel KI. 2019. Encoding of Wind Direction by Central Neurons in Drosophila. *Neuron* **102**:828–842.e7.

Takemura S, Aso Y, Hige T, Wong A, Lu Z, Xu CS. 2017. A connectome of a learning and memory center in the adult Drosophila brain. *Elife*.

Tanaka NK, Tanimoto H, Ito K. 2008. Neuronal assemblies of the Drosophila mushroom body. *J Comp Neurol* **508**:711–755.

Truman JW, Price J, Miyares RL, Lee T. 2022. Metamorphosis of memory circuits in Drosophila reveal a strategy for evolving a larval brain. *bioRxiv*. doi:10.1101/2022.06.09.495452

Tully T, Quinn WG. 1985. Classical conditioning and retention in normal and mutant Drosophila melanogaster. *J Comp Physiol A* **157**:263–277.

Tye KM. 2018. Neural Circuit Motifs in Valence Processing. *Neuron* **100**:436–452.

van Breugel F, Dickinson MH. 2014. Plume-tracking behavior of flying Drosophila emerges from a set of distinct sensory-motor reflexes. *Curr Biol* **24**:274–286.

Vergassola M, Villermaux E, Shraiman BI. 2007. “Infotaxis” as a strategy for searching without gradients. *Nature*. doi:10.1038/nature05464

Vet LEM, Van Lenteren JC, Heymans M, Meelis E. 1983. An airflow olfactometer for measuring olfactory responses of hymenopterous parasitoids and other small insects. *Physiological Entomology*. doi:10.1111/j.1365-3032.1983.tb00338.x

Vogt K, Aso Y, Hige T, Knapek S, Ichinose T, Friedrich AB, Turner GC, Rubin GM, Tanimoto H. 2016. Direct neural pathways convey distinct visual information to Drosophila mushroom bodies. *Elife* **5**. doi:10.7554/eLife.14009

Vogt K, Schnaitmann C, Dylla KV, Knapek S, Aso Y, Rubin GM, Tanimoto H. 2014. Shared mushroom body circuits underlie visual and olfactory memories in Drosophila. *Elife* **3**:e02395.

Wan Y, Otsuna H, Chien C-B, Hansen C. 2012. FluoRender: An Application of 2D Image Space Methods for 3D and 4D Confocal Microscopy Data Visualization in Neurobiology Research. *IEEE Pac Vis Symp* 201–208.

Yamada D, Bushey D, Feng L, Hibbard K, Sammons M, Funke J, Litwin-Kumar A, Hige T, Aso Y. n.d. Hierarchical architecture of dopaminergic circuits enables second-

order conditioning in *Drosophila*. doi:10.1101/2022.03.30.486484
Yamagata N, Ichinose T, Aso Y, Plaçais P-Y, Friedrich AB, Sima RJ, Preat T, Rubin GM, Tanimoto H. 2015. Distinct dopamine neurons mediate reward signals for short- and long-term memories. *Proc Natl Acad Sci U S A* **112**:578–583.
Yorozu S, Wong A, Fischer BJ, Dankert H, Kernan MJ, Kamikouchi A, Ito K, Anderson DJ. 2009. Distinct sensory representations of wind and near-field sound in the Drosophila brain. *Nature* **458**:201–205.
Zhang X, Li B. 2018. Population coding of valence in the basolateral amygdala. *Nat Commun* **9**:1–14.
Zhao T, Olbris DJ, Yu Y, Plaza SM. 2018. NeuTu: Software for Collaborative, Large-Scale, Segmentation-Based Connectome Reconstruction. *Front Neural Circuits* **12**:101.
Zheng Z, Lauritzen JS, Perlman E, Robinson CG, Nichols M, Milkie D, Torrens O, Price J, Fisher CB, Sharifi N, Calle-Schuler SA, Kmecova L, Ali IJ, Karsh B, Trautman ET, Bogovic JA, Hanslovsky P, Jefferis GSXE, Kazhdan M, Khairy K, Saalfeld S, Fetter RD, Bock DD. 2018. A Complete Electron Microscopy Volume of the Brain of Adult Drosophila melanogaster. *Cell* **174**:730–743.e22.
Zolin A, Cohn R, Pang R, Siliciano AF, Fairhall AL, Ruta V. 2021. Context-dependent representations of movement in Drosophila dopaminergic reinforcement pathways. *Nat Neurosci* **24**:1555–1566.

Figure Legends

Figure 1. Memories in specific set of MB-compartments drive upwind locomotion

(A) A conceptual diagram of the mushroom body circuit. The colored rectangles represent individual MB compartments.
(B) A diagram of a four-armed olfactory arena. In each experiment, approximately 20 female flies were introduced into the circular arena.
(C) Protocols for optogenetic training and the two different memory tests used in this work.
(D) Appetitive memories assessed by binary choice between CS+ and CS- odors immediately after training with optogenetic activation of DANs that express CsChrimson with drivers indicated in E. N=14-24.
(E) Time course of the area normalized mean of fly's position relative to the center of the arena as compared with its mean position at odor onset and the cosine of the angle between the fly's orientation and the upwind direction (See Methods). Flies of each genotype were trained with three protocols: 1) Pentyl Acetate (PA) was paired with the LED activating illumination and Ethyl Lactate (EL) was unpaired. 2) EL was paired with LED and PA was unpaired. 3) Neither odor was paired (No LED). Lines and filled areas around lines are mean and SEM. N=24-60.
(F) The delta of distance from the center at the end of the 10s odor period. Each dot represents data from individual trials. Black lines are mean and SEM. *, $p<0.05$; ***, $p<0.001$; Dunn's multiple comparison tests compared to empty-split-GAL4 control, following Kruskal-Wallis test; N=24-60. The upwind displacements of MB213B and MB043C in response to CS+ odor were also significantly higher than the control when trial averages of 6 movies were compared.

989 (G) Cumulative angle of turning and forward walking speed during the first 10 frames
990 (333ms; a time window we used for optogenetic experiments in Figure 6) following odor
991 onset are plotted against initial angle to upwind, smoothened with +/- 30-degree bin. The
992 number of trajectories analyzed for (CS+, CS-, No LED) conditions for
993 MB109B+MB315C, MB312C, MB213B and MB043C were (531, 562, 167), (710, 758,
994 814), (920, 1039, 919) and (449, 768, 531), respectively. Only flies that were 3mm or
995 more from the edge of the arena were analyzed.
996 (H) The violin-plots of the cumulative angle of turn to the upwind orientation during the
997 first 10 frames (333ms) of odor onset. Only flies that oriented -90 to -150 or +90 to 150
998 degrees to the upwind direction at odor onset were analyzed. N=122, 137, 233, 239, 99
999 for empty-split-GAL4, MB109B+MB315C, MB312C, MB213B and MB043C, respectively.
1000 *, $p<0.05$; ***, $p<0.001$; Dunn's multiple comparison tests compared to empty-split-GAL4
1001 control, following Kruskal-Wallis test.
1002
1003 **Figure 1-figure supplement 1. Memory-based modulation of walking speed and**
1004 **angular speed depends on the fly's initial angle to the upwind direction**

1005 (A-E) The cosine of the angle to upwind direction, angular speed and forward walking
1006 speed are separately plotted for flies oriented downwind or upwind at odor onset (Time =
1007 0 s). Only flies that were at least 3 mm away from the edge of the arena were analyzed.
1008 The source data are identical to Figure 1E-H.
1009
1010 **Figure 2. Identification of UpWiNs by activation screening**

1011 (A) Mean displacement of fly's position relative to the center of the arena during
1012 activation of various cell types defined by the indicated driver lines. Dunn's multiple
1013 comparison tests compared to empty-split-GAL4 control, following Kruskal-Wallis test;*,
1014 $p<0.05$; **, $p<0.01$; ***, $p<0.001$, N=18-132; Black asterisks indicate $p<0.05$ without
1015 correction for multiple comparisons. The median, first and third quartiles, 10 and 90
1016 percentiles are displayed with outlier data points. See Figure 2-figure supplement 1 and
1017 http://www.janelia.org/split-gal4 for expression patterns of CsChrimson in these driver
1018 lines.

1019 (B) Z-scores for five parameters for 2s time bins (T1 to T2) before, during (bold
1020 numbers) and after the 10s activation period. For calculating the probability of return,
1021 15s long trajectories of each fly following each time point (t1) were analyzed. A fly was
1022 considered to revisit the original location at time0 if it moved away more than 10mm and
1023 came back to within 3mm distance from that location at time0 within 15s. High Z-score at
1024 8-10s time bin indicate that flies tended to move back to their location at 8-10s by 23-25s
1025 (i.e. mostly dark period after LED was turned off).

1026 **Figure 2-figure supplement 1. Activation phenotypes of "hit" lines**

1027 Time courses of five behavioral parameters are shown for driver lines with significant
1028 upwind locomotion (i.e. delta distance from center) phenotypes in Figure 2. Lines and
1029 shaded areas around lines are mean and SEM; split-GAL4>CsChrimson-mVenus are
1030 shown in blue and empty-split-Gal4>CsChrimson-mVenus in gray.

1031 **Figure 2-figure supplement 2. Expression patterns of "hit" lines**

1032 Projection of confocal microscopy stacks for expression patterns of CsChrimson-
1033 mVenus driven by designated split-GAL4 driver lines in brains and ventral nerve cords.

1034 Confocal stacks are available at https://splitgal4.janelia.org

1035 **Figure 2-figure supplement 3. LM-EM matching of cell types in SS49899**

1036 (A) The fan-shaped body neurons in SS49899 driver that were visualized with myr-
1037 smGFP-HA (green) and synaptotagmin-smGFP-V5 (magenta). The outlines of the
1038 standard brain and the mushroom body are shown in gray. Other driver lines with similar
1039 expression patterns are listed.

1040 (B) The corresponding EM reconstructed neurons, which were matched by comparing
1041 projection patterns in the standard brain and referring MCFO images of split-GAL4.
1042 Confocal stacks are available at https://splitgal4.janelia.org

1043 **Figure 2-figure supplement 4. LM-EM matching of cell types in SS49755**

1044 (A) The SMP neurons in SS49755 driver that were visualized with myr-smGFP-HA
1045 (green) and synaptotagmin-smGFP-V5 (magenta). The outlines of the standard brain
1046 and the mushroom body are shown in gray. Other driver lines with similar expression
1047 patterns are listed.

1048 (B) The corresponding EM reconstructed neurons, which were matched by comparing
1049 projection patterns in the standard brain and referring MCFO images of split-GAL4.
1050 Confocal stacks are available at https://splitgal4.janelia.org

1051

1052 **Figure 3. Connectivity of UpWiNs**

1053 (A) The expression pattern of CsChrimson-mVenus driven by split-GAL4 line SS33917.

1054 (B) Eleven EM-reconstructed neurons that correspond to UpWiNs defined by the
1055 SS33917 driver were identified by analyzing the morphology of individual neurons
1056 (Figure 3-figure supplement 1 and 2) and are displayed with outline of the MB and the
1057 standard brain. Individual neurons are color-coded to indicate the cell type to which they
1058 were assigned.

1059 (C) Connectivity of UpWiNs with major upstream and downstream neurons that have at
1060 least 20 connections with one of the 11 UpWiNs. The hemibrain bodyIDs of each neuron
1061 is shown as well as their assignment to specific cell types. Numbers indicate the number
1062 of synapses from the upstream neurons to UpWin neurons (left) or from the UpWiNs to
1063 the downstream neurons (right).

1064 (D) Interneurons downstream to MBON-α1 and MBON-α3. Colors of dots indicate
1065 neurotransmitter prediction (Eckstein et al., n.d.). See Figure 3-figure supplement 3 for
1066 more detail.

1067 (E) Predicted postsynaptic sites in SMP353 and SMP354 (gray), which are juxtaposed to
1068 presynaptic sites from MBON-α1 (green) and MBON-α3 (orange).

1069 (F) Interconnectivity between UpWiNs. The numbers indicate the summed number of
1070 connections. The numbers in parentheses indicate the number of neurons per cell type.

1071

Figure 3-figure supplement 1. Candidate UpWiNs in hemibrain EM images

(A) Frontal and dorsal projection of 11 EM-reconstructed neurons that were matched with confocal images of UpWiNs within the standard brain (Bogovic et al., 2020) (see Figure 3-figure supplement 2). Pseudo colors were assigned to each of five cell types. The arrowhead and arrow indicate common axonal tract and terminal area in the SMP. IDs of each neuron are displayed. The somas of these neurons are clustered near the tip of the vertical lobe of the MB, and they share the tracts for the primary neurite and axons, whereas the branching patterns of their dendrites exhibit cell-type-specific characteristics, which were used for cell type matching.
(B-L) Projections of individual neurons. The arrows indicate dendritic branches that are characteristic to each cell type.

Figure 3-figure supplement 2. Single cell images of neurons in SS33917

(A-Y) Frontal projections of segmented multi-color flp-out images of SS33917 (colored) with corresponding EM neuron (gray). The arrows indicate dendritic branches that are characteristic to each cell type.

Figure 3-figure supplement 3. NBLAST clustering of single cell images of neurons in SS33917

MCFO single cell images of SS33917 driver were clustered into 6 groups, which were nearly identical to the manual annotation.

Figure 3-figure supplement 4. Downstream neurons of MBON-α1 and MBON-α3

Connectivity from MBON-α1 and MBON-α3 to downstream neurons that receive at least 10 connections.

Figure 4. UpWiNs integrate excitatory and inhibitory synaptic inputs from MBONs.
(A) Functional connectivity between MBON-α3 and UpWiNs. Chrimson88-tdTomato was expressed in MBON-α3 by MB082C split-GAL4, and the photostimulation responses were measured by whole-cell current-clamp recording in randomly selected UpWiNs labeled by R64A11-LexA. 2 out of 6 neurons (4 flies) showed excitatory response. Mean voltage traces from individual connected (orange) and unconnected UpWiNs (gray) are overlaid. The connection was strong enough to elicit spikes (black; single-trial response in one of the connected UpWiNs). Magenta vertical line indicates photostimulation (10 msec).
(B) Functional connectivity between MBON-α1 and UpWiNs. Chrimson88-tdTomato expression in MBON-α1 was driven by MB310C split-GAL4. 4 out of 17 neurons (12 flies) showed inhibitory response. Mean voltage traces from individual connected (green) and unconnected UpWiNs (gray) are overlaid.
(C) Integration of synaptic inputs from MBON-α3 and MBON-α1. Population responses of UpWiNs were measured by two-photon calcium imaging at the junction between dendrites and axonal tracts (mean $\Delta F/F \pm$ SEM) while photostimulating MBON-α3 (orange; n = 5), MBON-α1 (green; n = 11) or both (black; n = 7). Expression of GCaMP6s was driven by R64A11-LexA, and Chrimson88-tdTomato by G0239-GAL4

(MBON-α3) and/or MB310C (MBON-α1). Photostimulation: 1 sec (magenta). While activation of MBON-α1 did not evoke detectable inhibition in the calcium signal, it effectively canceled the excitation by MBON-α3.

Figure 5. Optogenetic appetitive conditioning enhances the response to the conditioned odor in UpWiNs.
(A) Optogenetic conditioning was performed by pairing photostimulation of PAM-DANs with odor presentation. Expression of ChrimsonR-mVenus was driven by 58E02-LexA, and in vivo whole-cell recordings were made from UpWINs labeled by GFP using SS67249-split-GAL4. 1-min presentation of OCT was paired with LED stimulation (1 ms, 2 Hz, 120 times), followed by 1-min presentation of MCH alone.
(B) Representative recording from a single fly. Gray bars indicate 1-s odor presentation.
(C) Mean (± SEM) odor responses (n = 6). Spikes were removed by a low-pass filter.
(D) Summary data of mean (± SEM) odor-evoked membrane depolarization. Gray lines indicate data from individual neurons. Responses to OCT were potentiated ($p < 0.01$; repeated-measures two-way ANOVA followed by Tukey's post hoc multiple comparisons test), while those to MCH did not change ($p = 0.9$).

Figure 5 – figure supplement 1. Expression patterns of SS67249
(A) Expression of CsChrimson-mVenus driven by SS67249.
(B-D) MCFO image of neurons in SS67249 (red) and SMP353 (gray) with outline of the MB and the standard brain.

Figure 5 – figure supplement 2. Reciprocal experiment of optogenetic appetitive conditioning.
(A) Experimental design and protocol. Same as Figure 5 except that MCH was paired with DAN photostimulation.
(B) Representative recording from a single fly. Gray bars indicate 1-s odor presentation.
(C) Mean (± SEM) odor responses (n = 5). Spikes were removed by a low-pass filter.
(D) Summary data of mean (± SEM) odor-evoked membrane depolarization. Gray lines indicate data from individual neurons. Responses to MCH were potentiated ($p < 0.001$; repeated-measures two-way ANOVA followed by Tukey's post hoc multiple comparisons test), while those to OCT did not change ($p = 0.4$).

Figure 6. Activity of UpWiNs bias turning direction
(A) Fed or 40-48 hours starved flies were compared to assess requirement of starved status for UpWiNs to promote upwind locomotion. N=14 (fed) and 16 (starved); ***, $p<0.001$, Mann-Whitney test;
(B) Upwind locomotion during the 10s activation of UpWiNs in the arena with various rates of airflow. N=9-16;**, $p<0.01$; Dunn's multiple comparison tests compared to the zero flow condition.
(C) Right side or both sides of aristae were ablated one-day prior to experiments to measure upwind response during UpWiN activation. N=20 (intact) and 40 (unilateral and bilateral); ***, $p<0.001$; Dunn's multiple comparison tests compared to the intact control.
(D) Behavioral kinematics of UpWiN activation. The trajectories of individual flies during first 1.5s of 10s LED period were grouped to initially facing downwind or upwind if cos(upwind angle) was above 0.5 or below -0.5, respectively.
(E) Cumulative angle of turning and forward walking speed during the first 10 frames (333ms) after the onset of LED plotted against initial angle to upwind smoothened with +/- 30 degree bin. The number of trajectories analyzed for (SS33917, SS33918,

MB077B, Empty-split-GAL4) were (2492, 3362, 772, 1582), respectively. Only flies that were at least 3mm away from the edge of the arena were analyzed.
(F-G) The violin-plots of the cumulative angle of turn to the upwind orientation or forward walking speed during the first 10 frames (333ms) of odor onset. Only flies that oriented -90 to -150 or +90 to 150 degrees to upwind at the odor onset were analyzed. N=444, 540, 231, 219 for SS33917, SS33918, MB077B, Empty-split-GAL4, respectively. **, $p<0.01$; ***, $p<0.001$; Dunn's multiple comparison for the selected pairs, following Kruskal-Wallis test.

Figure 6-figure supplement 1
(A-E) The cosine of angle to upwind, angular speed and forward walking speed are separately plotted for flies oriented downwind or upwind at the odor onset. Only flies that were 3mm away from the edge of the arena were analyzed. The source data are identical to Figure 2.

Figure 7. UpWiNs are required for memory-driven upwind locomotion
(A) Upwind response to the odor associated with sugar in control genotypes and flies that express TNT in UpWiNs.
(B) Time course of upwind response.
(C) Appetitive memories of control genotypes and flies expressing shibire in UpWiNs were tested one-day after odor-sugar conditioning at restrictive or permissive temperature.
(D) Time course of fly's preference to quadrants with red LED light by SS33917>CsChrimson (blue) or empty-split-GAL4>CsChrimson (gray). The preference to red LED quadrants during the last 5s of two 30s activation period was significantly higher for SS33917>CsChrimson flies (right).
(E) The probability of returning to the location where LED stimulation was terminated were measured as in Figure 2, but without airflow. See Figure 7-figure supplement 1 for the time courses and other parameters. UpWiN drivers are shown together with SS49755 from the screen.

Figure 7-figure supplement 1 UpWiN activation phenotypes without airflow
Time course of the five parameters shown in Figure 2-figure supplement 1 but in the absence of airflow. Lines and filled areas around lines are mean and SEM; CsChrimson-expressing flies (blue) and empty-split-GAL4 control (gray).

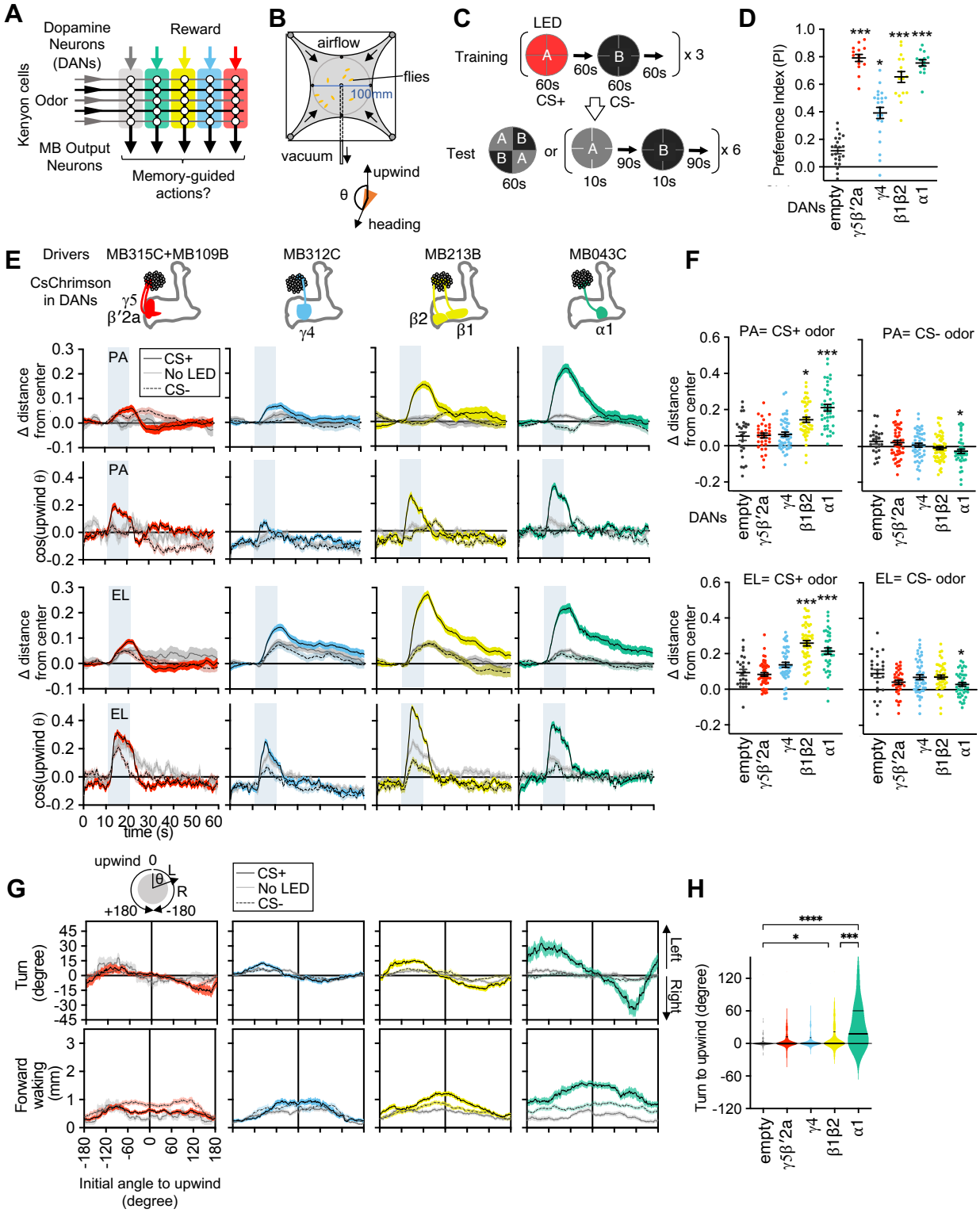
A
Dopamine Neurons (DANs)
Reward
Kenyon cells
Odor
MB Output Neurons
Memory-guided actions?
B
airflow
flies
100mm
vacuum
upwind
θ
heading
C
LED
Training
A
B
60s
60s
60s
x 3
CS+
CS-
Test
A B
B A
60s
or
A
B
90s
90s
10s
10s
x 6
D
Preference Index (PI)
DANs
empty
γ5β′2a
γ4
β1β2
α1
E
Drivers
MB315C+MB109B
MB312C
MB213B
MB043C
CsChrimson in DANs
γ5
β′2a
γ4
β2
β1
α1
PA
EL
CS+
No LED
CS-
Δ distance from center
cos(upwind θ)
time (s)
F
PA= CS+ odor
PA= CS- odor
EL= CS+ odor
EL= CS- odor
G
upwind 0
L
R
+180
-180
Turn (degree)
Forward waking (mm)
Left
Right
Initial angle to upwind (degree)
H
Turn to upwind (degree)

Figure 1

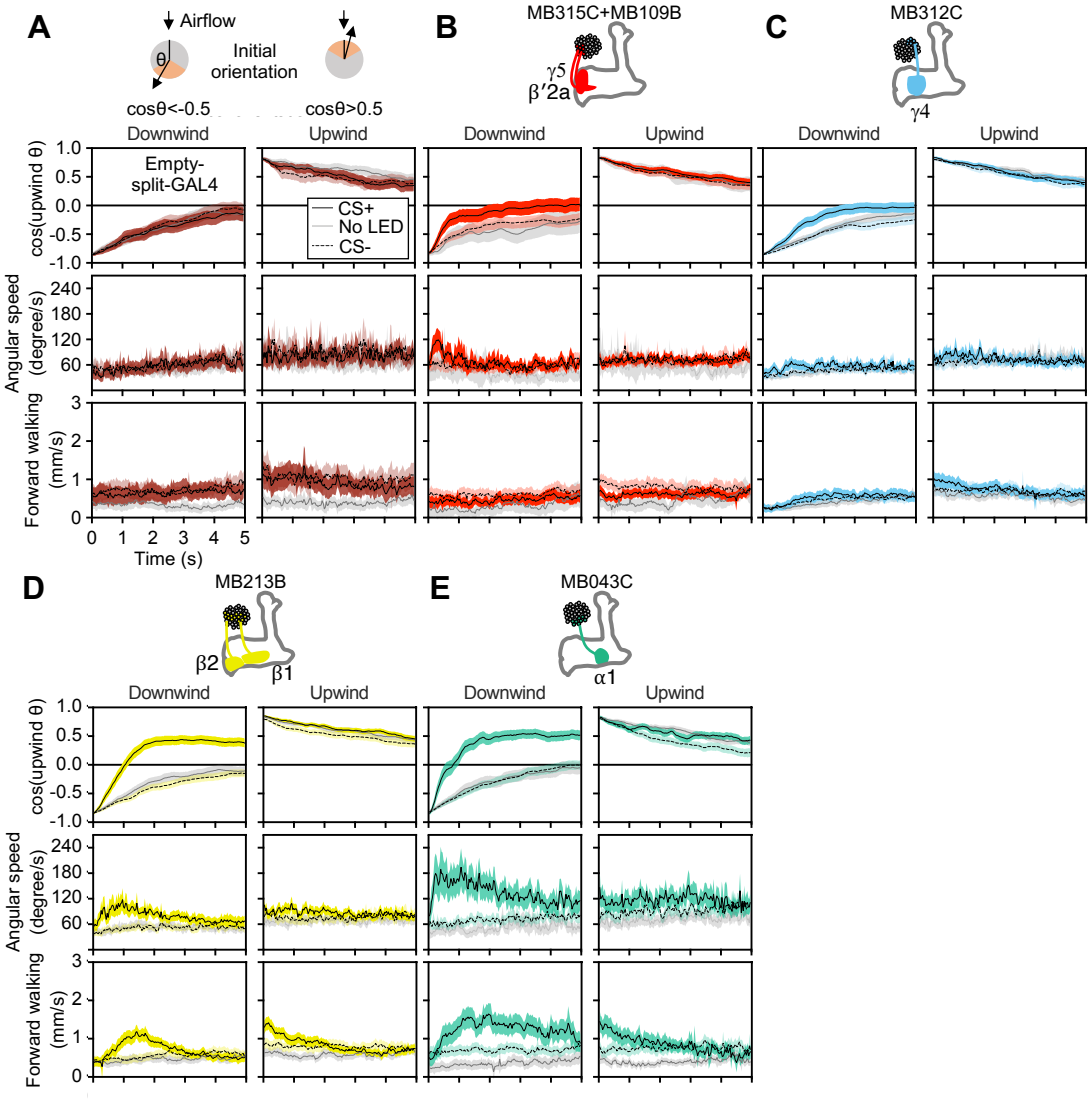

Figure 1-figure supplement 1

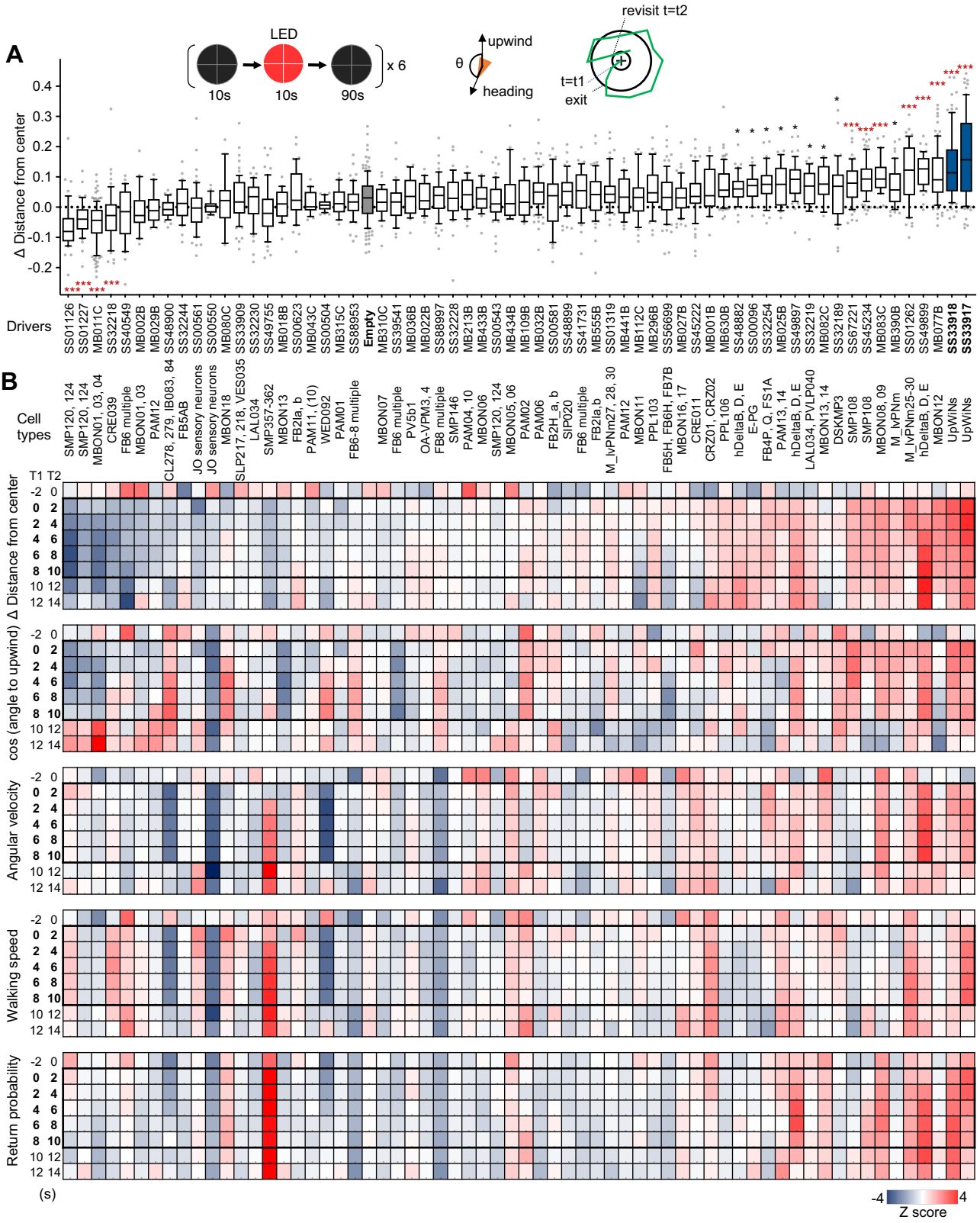
A
LED
10s
10s
90s
x 6
θ
upwind
heading
revisit t=t2
t=t1
exit
Δ Distance from center
Drivers
B
Cell types
T1 T2
Δ Distance from center
cos (angle to upwind)
Angular velocity
Walking speed
Return probability
(s)
-4
4
Z score

Figure 2

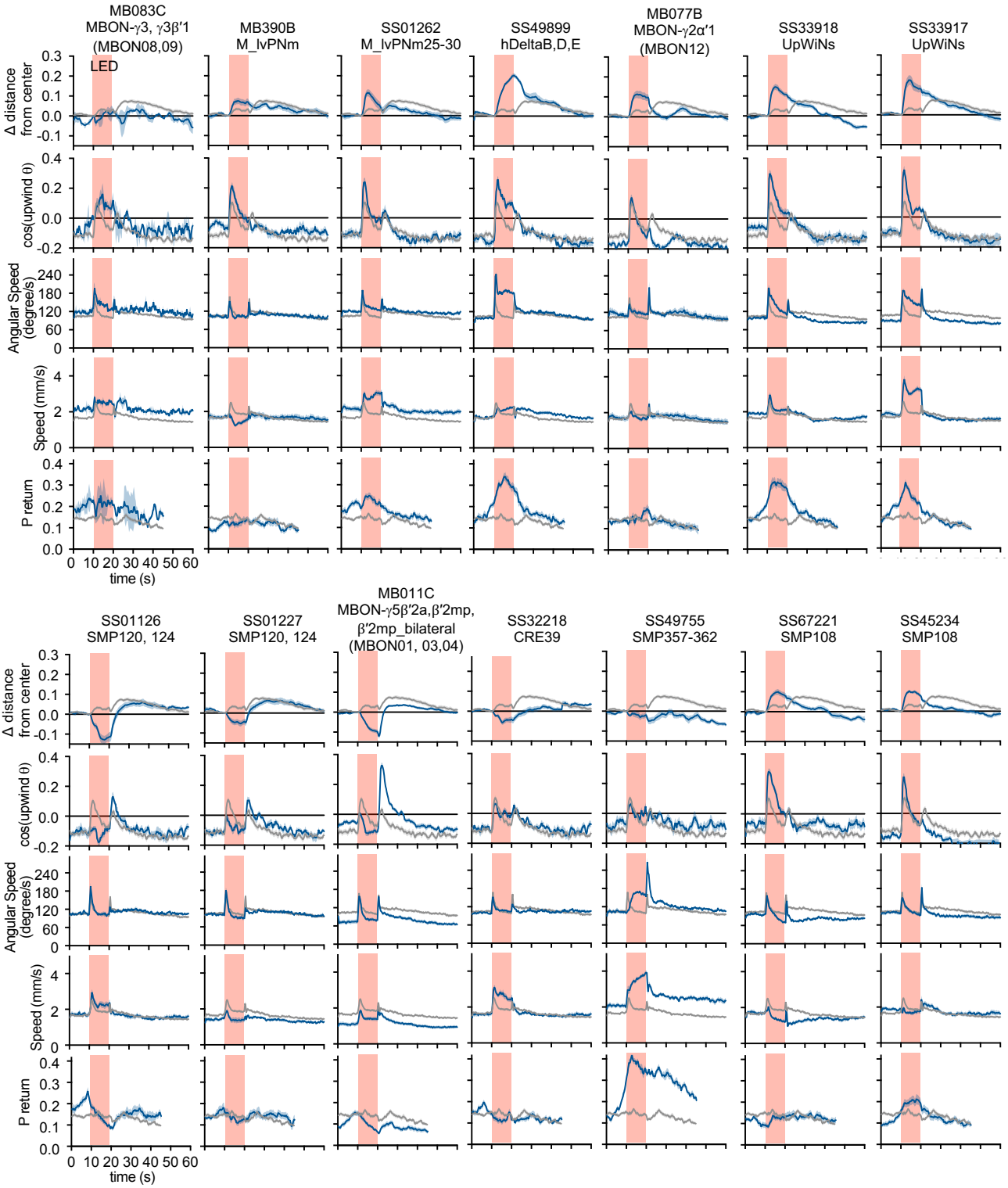

Figure 2-figure Supplement 1

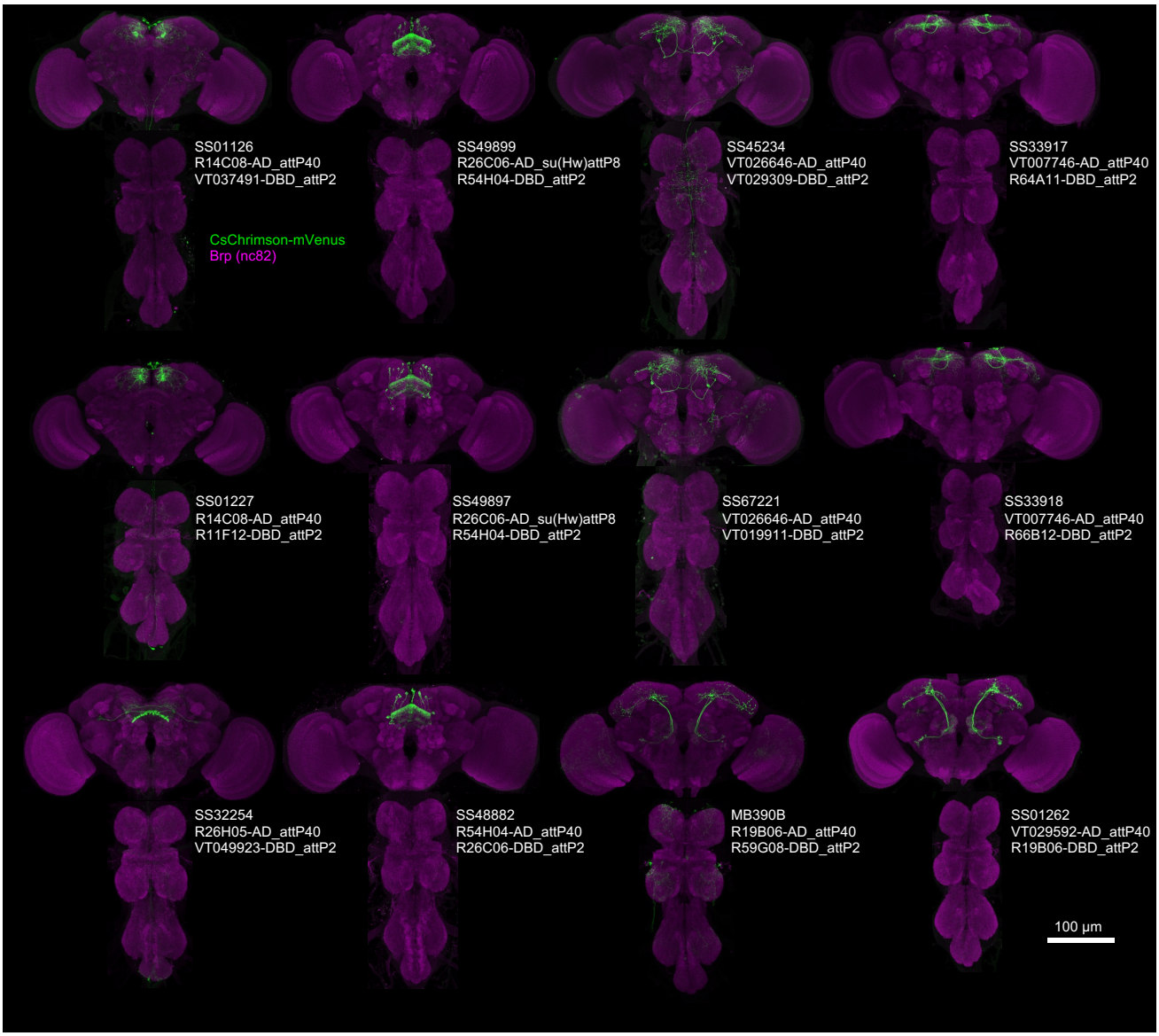

Figure 2-figure Supplement 2

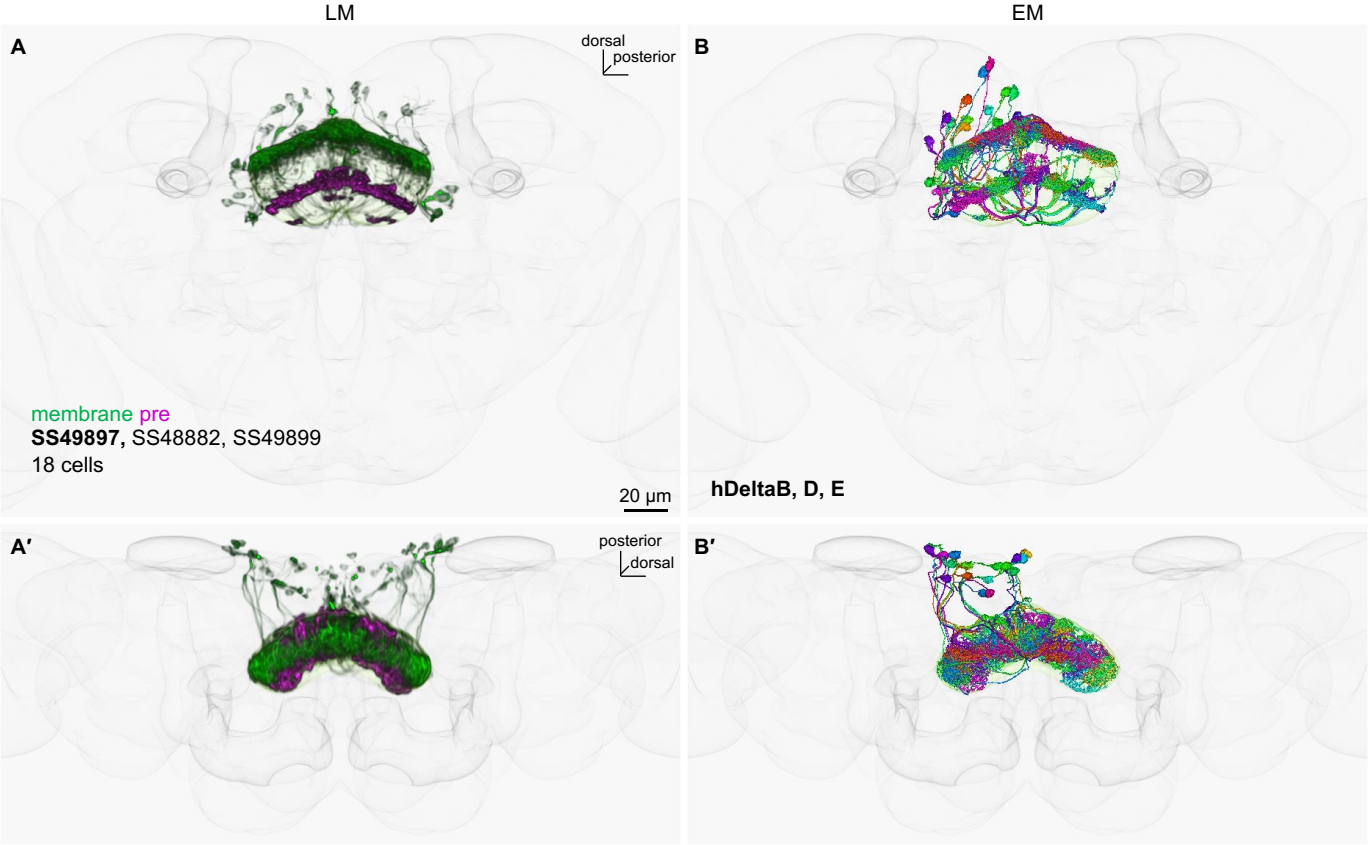

Figure 2-figure Supplement 3

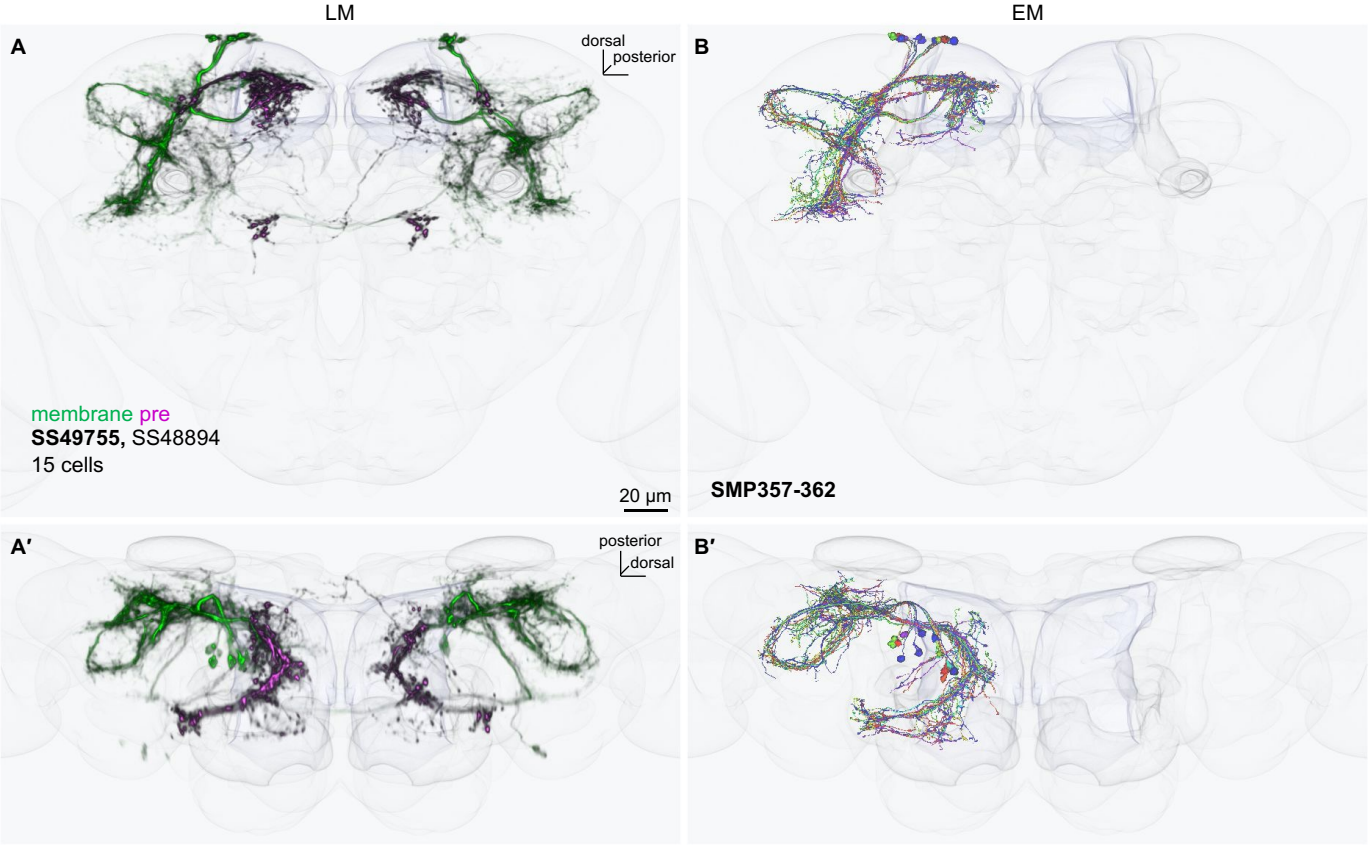

Figure 2-figure Supplement 4

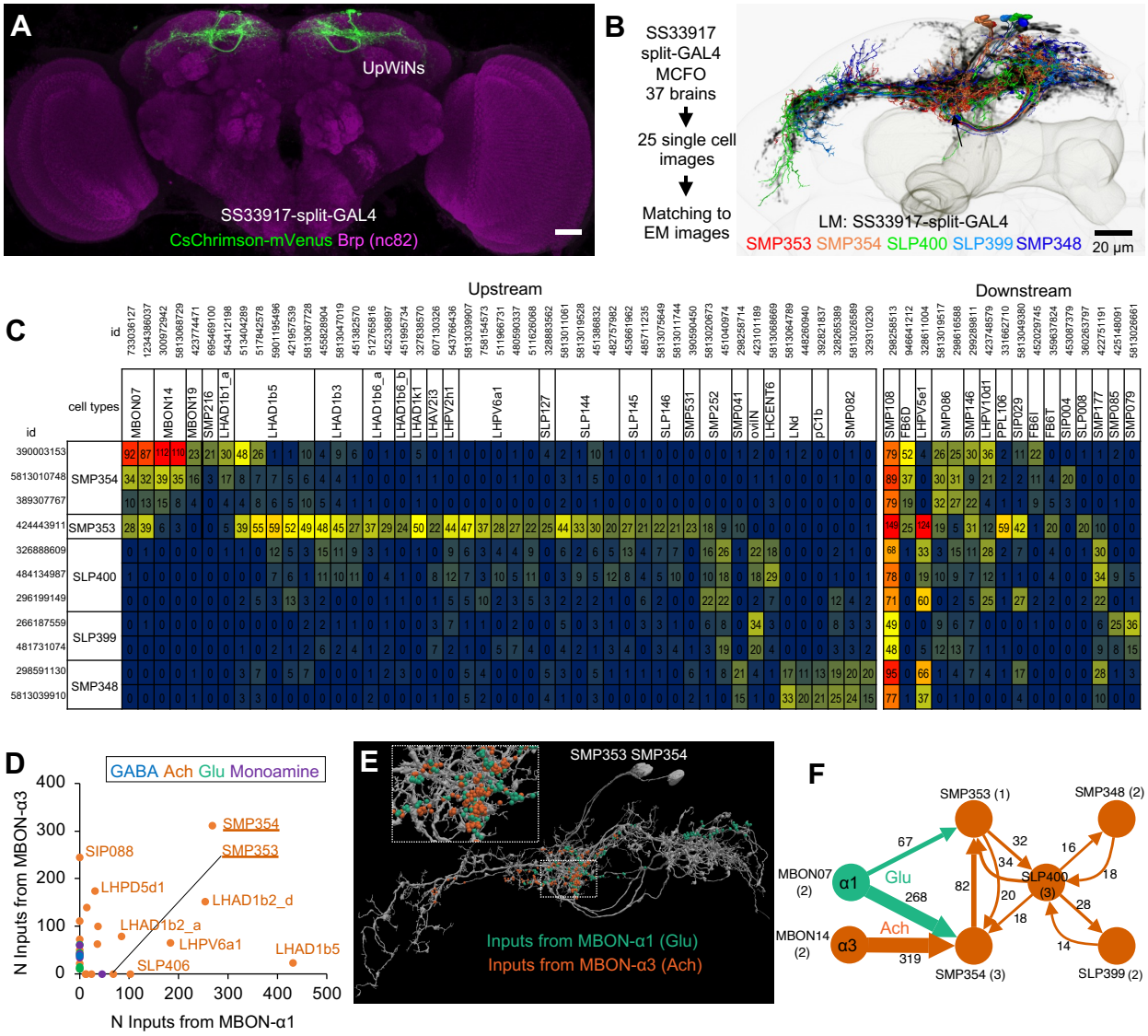
A
UpWiNs
SS33917-split-GAL4
CsChrimson-mVenus Brp (nc82)
B
SS33917
split-GAL4
MCFO
37 brains
25 single cell
images
Matching to
EM images
LM: SS33917-split-GAL4
SMP353 SMP354 SLP400 SLP399 SMP348
20 µm
C
Upstream
Downstream
id
cell types
MBON07
MBON14
MBON19
SMP216
LHAD1b1_a
LHAD1b5
LHAD1b3
LHAD1b6_a
LHAD1b6_b
LHAD1K1
LHAV2l3
LHPV2h1
LHPV6a1
SLP127
SLP144
SLP145
SLP146
SMP531
SMP252
SMP041
ovlIN
LHCENT6
LNd
pC1b
SMP082
SMP108
FB6D
LHPV5e1
SMP086
SMP146
LHPV10d1
PPL106
SIP029
FB6I
FB6T
SIP004
SLP008
SMP177
SMP085
SMP079
SMP354
SMP353
SLP400
SLP399
SMP348
D
GABA Ach Glu Monoamine
N Inputs from MBON-α3
N Inputs from MBON-α1
SMP354
SMP353
SIP088
LHPD5d1
LHAD1b2_d
LHAD1b2_a
LHPV6a1
LHAD1b5
SLP406
E
SMP353 SMP354
Inputs from MBON-α1 (Glu)
Inputs from MBON-α3 (Ach)
F
SMP353 (1)
SMP348 (2)
MBON07
(2)
α1
Glu
MBON14
(2)
α3
Ach
SLP400
(3)
SMP354 (3)
SLP399 (2)

Figure 3

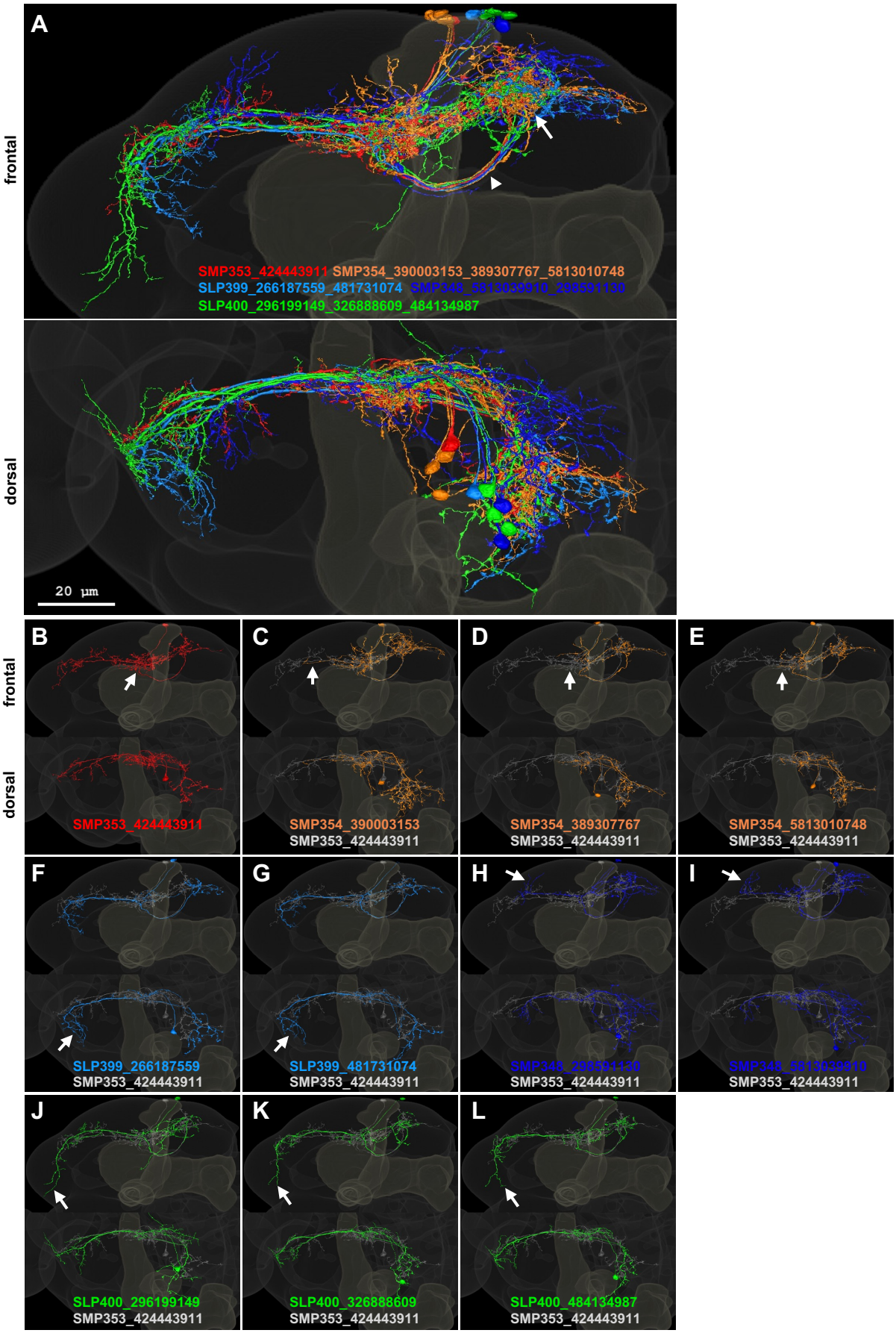

Figure 3-figure supplement 1

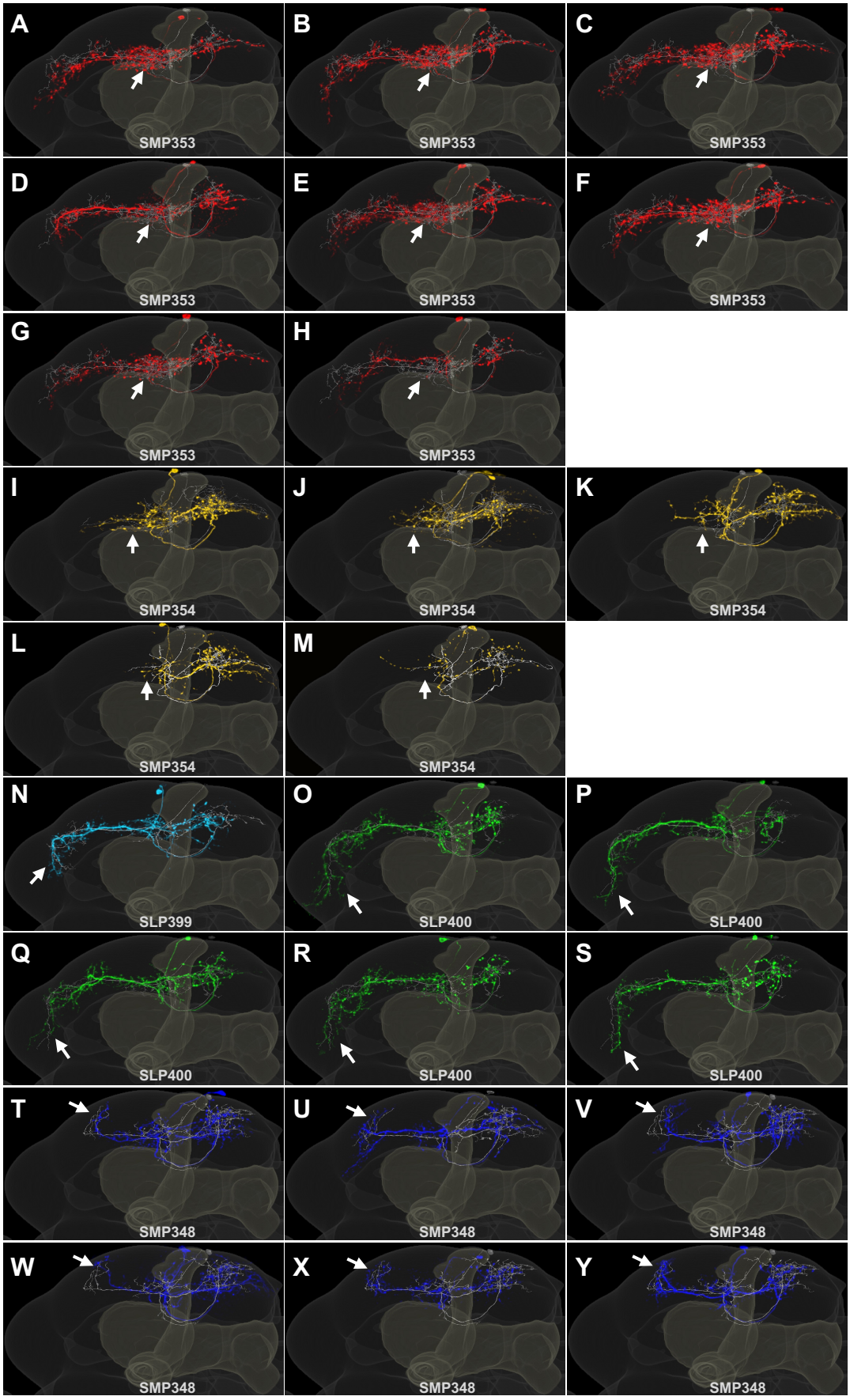

Figure 3-figure supplement 2

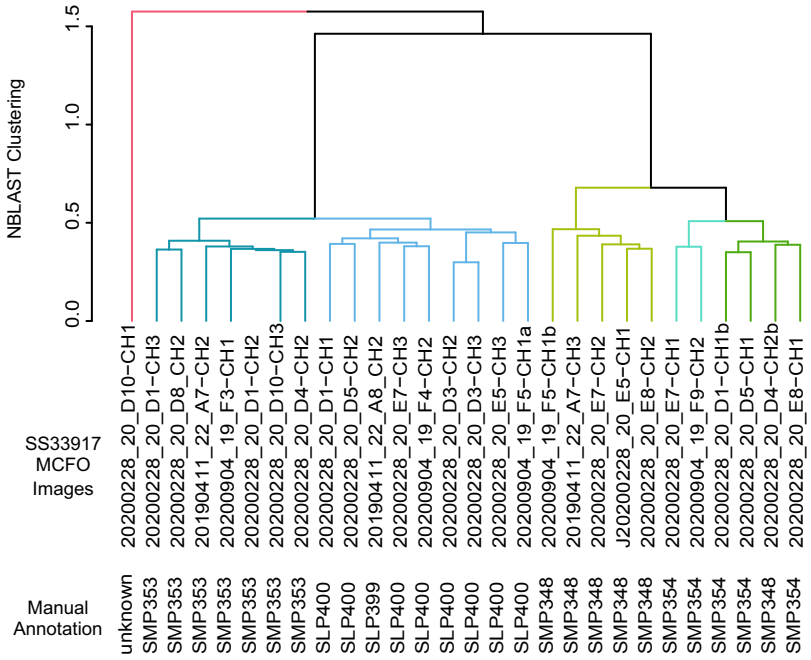

Figure 3-figure supplement 3

Cell type		MBON07	MBON14	MBON01	MBON12	MBON13	MBON02	MBON20	MBON18	MBON05	MBON06	MBON09	MBON19	MBON16	MBON11	MBON15-like	MBON17	MBON21	MBON15	MBON17-like	MBON04	MBON03	MBON10	
MB compartments		a1	a3	y5β'2a	γ2α'1	α'2	β2β'2a	γ1γ2	α2sc	γ4>γ1γ2	β1>α	γ3β'1	α2p3p	α'3ap	γ1pedc>α/β	α'1α'2	α'3m	γ4γ5	α'1	α'2α'3	β'2mp_bilateral	β'2mp	β'1	
Cell type	Transmitter	Glu	Ach	Glu	Ach	Ach	Glu	(GABA)	Ach	Glu	Glu	GABA	Ach	Ach	GABA	Ach	Ach	(Ach)	Ach	Ach	Glu	Glu	GABA	EM id
LHAD1b5	ACh	431	23	0	0	0	0	0	0	0	0	0	0	0	0	0	0	0	0	0	0	0	0	421957539, 513404289, 517842578, 5813067728, 5901195496,
SMP354	ACh	268	311	0	0	0	0	0	0	0	0	0	56	0	0	0	0	0	0	0	0	0	0	389307767, 390003153, 5813010748
LHAD1b2_d	ACh	253	152	258	59	53	13	0	0	10	0	0	0	0	0	0	0	0	0	0	0	0	0	544107243, 730562988
LHPV6a1	ACh	183	66	0	0	0	0	0	0	0	0	0	0	0	0	0	0	0	0	0	0	0	0	480590337, 480594756, 480599437, 480945354, 481627444, 511625768, 511626068, 511626286, 511966731, 543684107, 574468840, 5813012322, 5813039907, 758154573
SLP406	ACh	102	0	0	0	0	0	0	0	0	0	0	0	0	0	0	0	0	0	0	0	0	0	512377806
LHAD1b2_a	ACh	84	79	240	62	47	0	0	0	11	0	0	0	0	0	0	0	0	0	0	0	0	0	544107335, 5813013202, 606461310, 673426956, 769199010, 824349873
SMP353	ACh	67	0	0	0	0	0	0	0	0	0	0	0	0	0	0	0	0	0	0	0	0	0	424443911
PPM1201	DA	45	0	0	0	0	0	317	0	0	0	0	0	0	0	0	0	0	0	0	0	0	0	792040520, 950229431
SMP031	ACh	36	100	206	106	0	51	0	0	165	28	0	0	0	0	0	0	32	0	0	10	0	0	517838849, 579230376
LHAD1k1	ACh	35	63	0	0	0	0	0	0	0	0	0	0	0	0	0	0	0	0	0	0	0	0	327838570
LHPD5d1	ACh	30	174	231	53	0	41	0	0	0	0	86	0	0	0	43	0	0	11	11	0	0	0	387568523, 5813055800
LHAD1b6_a	ACh	23	0	11	0	0	0	0	0	0	0	0	0	0	0	0	0	0	0	0	0	0	0	425471220, 452336897, 512765816
LHAD1b3	ACh	14	140	0	0	0	0	0	0	0	0	0	0	0	0	0	0	0	0	0	0	0	0	451382570, 455828904, 5813047019
LHAD1b2_c	ACh	13	0	40	11	40	0	0	0	0	0	0	0	0	0	0	0	0	0	0	0	0	0	543321179, 574040939, 5813052205, 762274975
LHAD1b2_b	ACh	12	0	0	0	0	0	0	0	0	0	0	0	0	0	0	0	0	0	0	0	0	0	483017681, 573683438, 5813022459
SIP088	ACh	0	245	0	0	23	193	0	54	0	18	0	0	0	0	0	0	0	0	0	0	0	0	331011085
LHPV2h1	ACh	0	112	0	0	0	0	0	0	0	0	0	0	0	0	0	0	0	0	0	0	0	0	543766436
SMP549	ACh	0	73	0	12	0	0	0	0	0	18	0	0	0	0	0	0	0	0	0	0	0	0	329566197, 455229034
SIP016	Glu	0	62	0	53	114	0	0	0	0	0	0	0	50	0	0	10	0	0	0	0	0	0	518183562, 578893446, 579596940, 612648076
5-HTPMPD01	5-HT	0	61	0	0	10	0	0	15	0	0	0	0	0	0	0	0	0	0	0	0	0	0	297230760, 297908801
SLP391	ACh	0	51	0	0	0	0	0	0	0	58	0	0	0	0	0	0	0	0	0	0	0	0	298612190
SIP015	Glu	0	45	0	128	169	0	0	0	0	0	0	0	0	0	0	0	0	0	0	0	0	0	294450004, 486812022, 548203966, 549219101
SLP129_b	DA	0	42	0	0	0	0	0	0	0	0	0	0	0	0	0	0	0	0	0	0	0	0	392645419, 5813021223
SMP026	ACh	0	40	0	0	0	0	0	0	0	0	0	0	0	0	0	0	0	0	0	0	0	0	298599271, 5813068707
LHCENT9	GABA	0	38	33	0	0	96	0	145	0	48	0	16	0	11	0	25	0	0	0	0	0	0	330268940
SLP129_a	DA	0	35	0	0	0	0	0	0	0	0	0	0	0	0	0	0	0	0	0	0	0	0	5813012028
LHAV6a9	ACh	0	22	0	0	0	0	0	0	0	0	0	0	0	21	0	0	0	0	0	0	0	0	329581637, 360254511, 391954490
SMP170	Glu	0	15	0	0	0	0	0	0	0	0	0	0	0	0	0	0	0	0	0	0	0	0	299626157, 361700223
SMP194	ACh	0	11	0	23	0	0	0	0	0	0	0	0	0	12	0	0	0	0	0	0	0	0	613338546
SLP176	Glu	0	11	0	0	0	0	0	0	0	0	0	0	0	0	0	0	0	0	0	0	0	0	329566187, 389575937, 390969969, 419588136, 420952125, 5813010255

Figure 3 – figure supplement 4

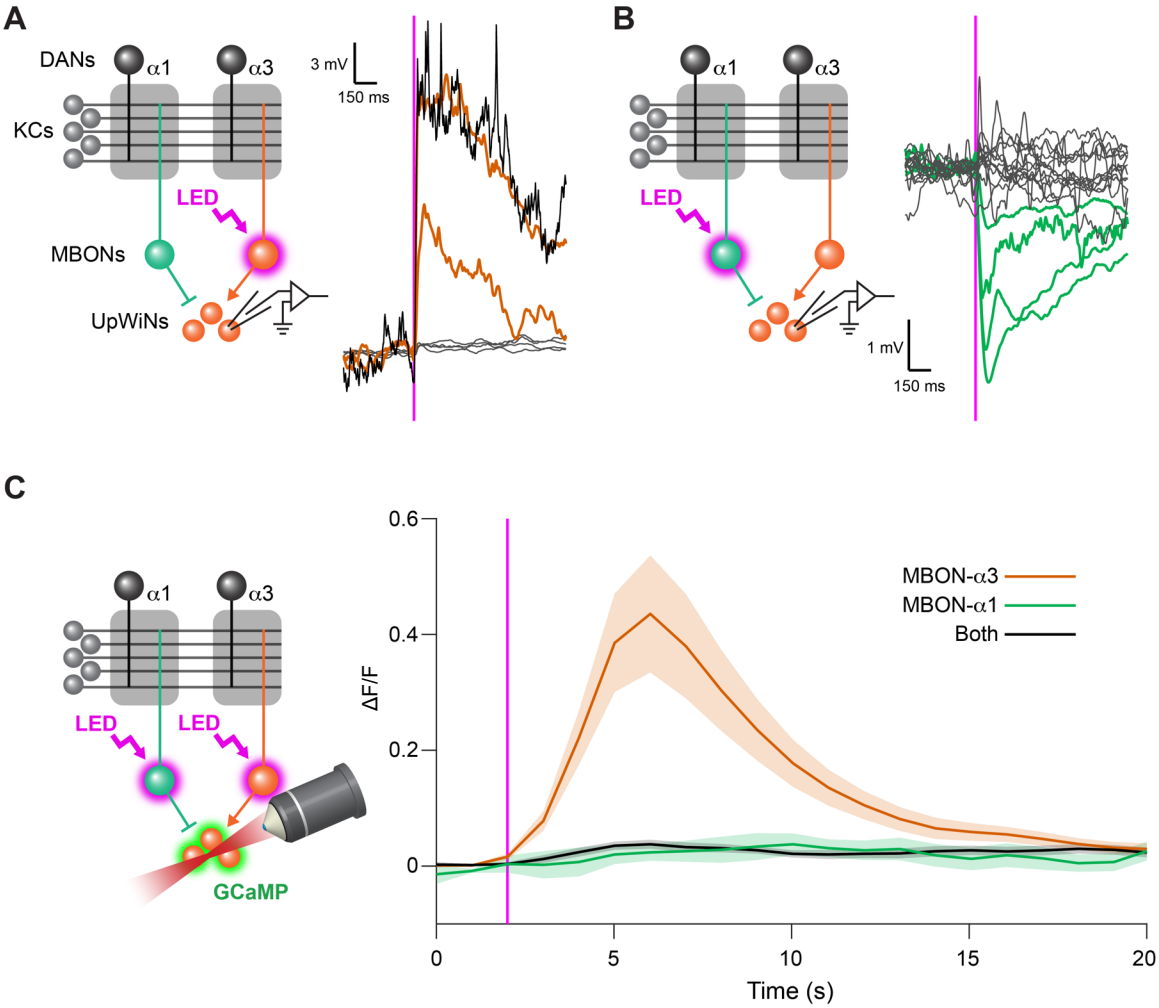
A
DANs
α1
α3
KCs
LED
MBONs
UpWiNs
3 mV
150 ms
B
α1
α3
LED
1 mV
150 ms
C
α1
α3
LED
LED
GCaMP
0.6
0.4
0.2
0
ΔF/F
MBON-α3
MBON-α1
Both
0
5
10
15
20
Time (s)

Figure 4

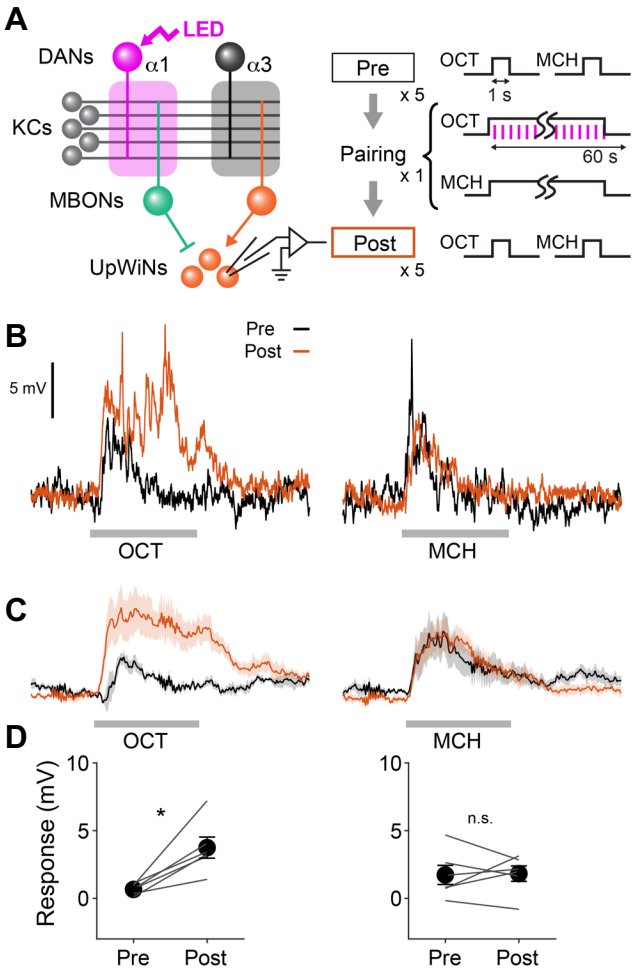
A
LED
DANs
α1
α3
KCs
MBONs
UpWiNs
Pre
x 5
Pairing
x 1
Post
x 5
OCT
MCH
1 s
60 s
B
Pre
Post
5 mV
OCT
MCH
C
OCT
MCH
D
Response (mV)
10
5
0
*
n.s.
Pre
Post

Figure 5

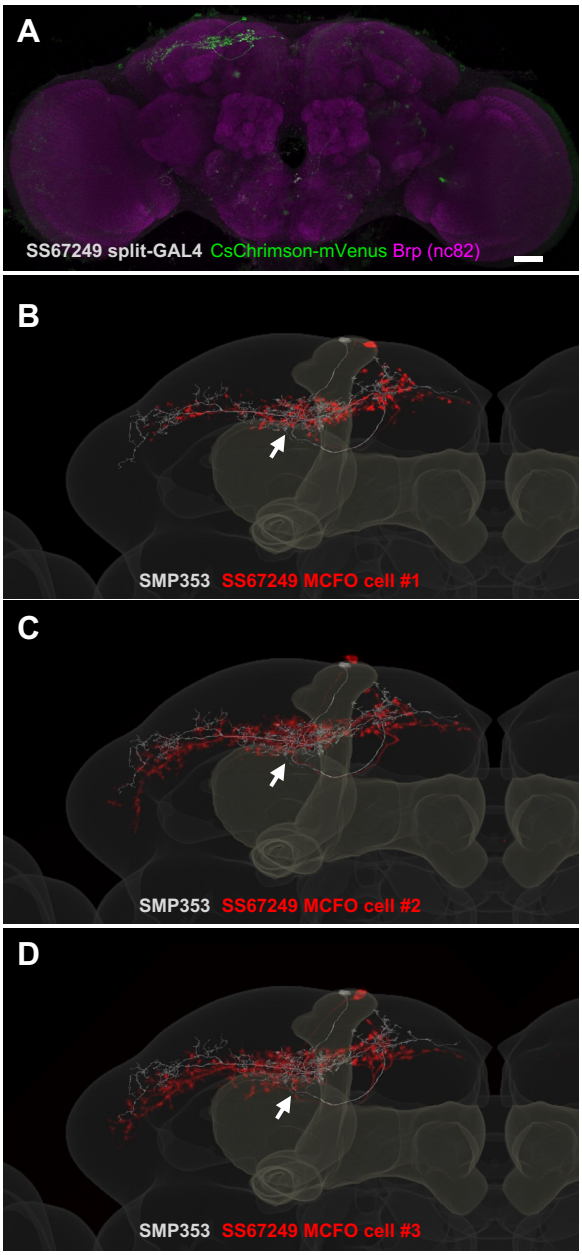

Figure 5 – figure supplement 1

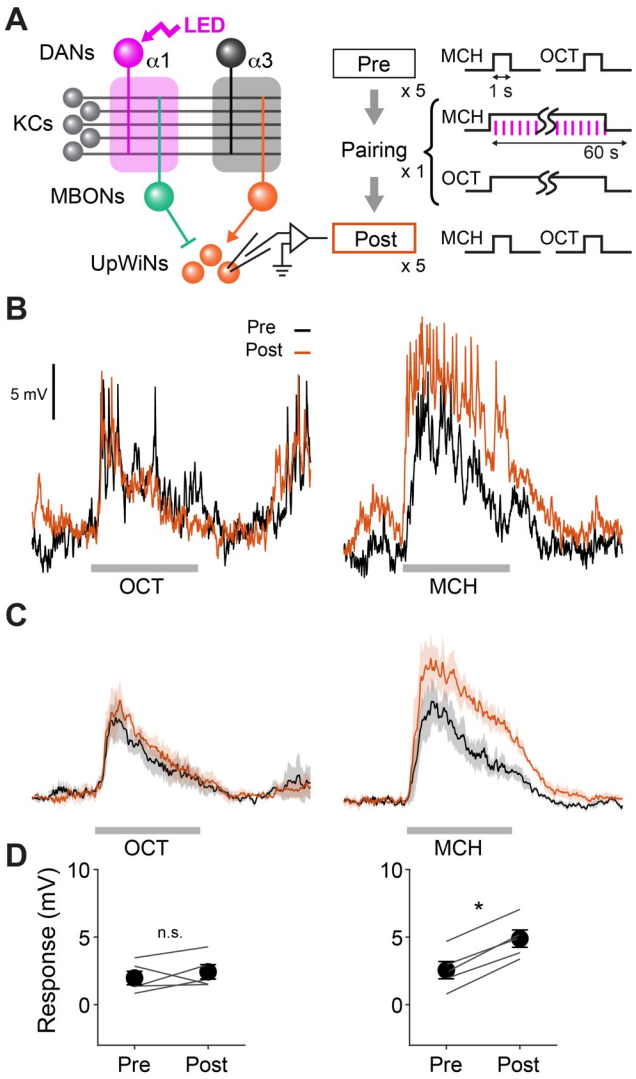

Figure 5 – figure supplement 2

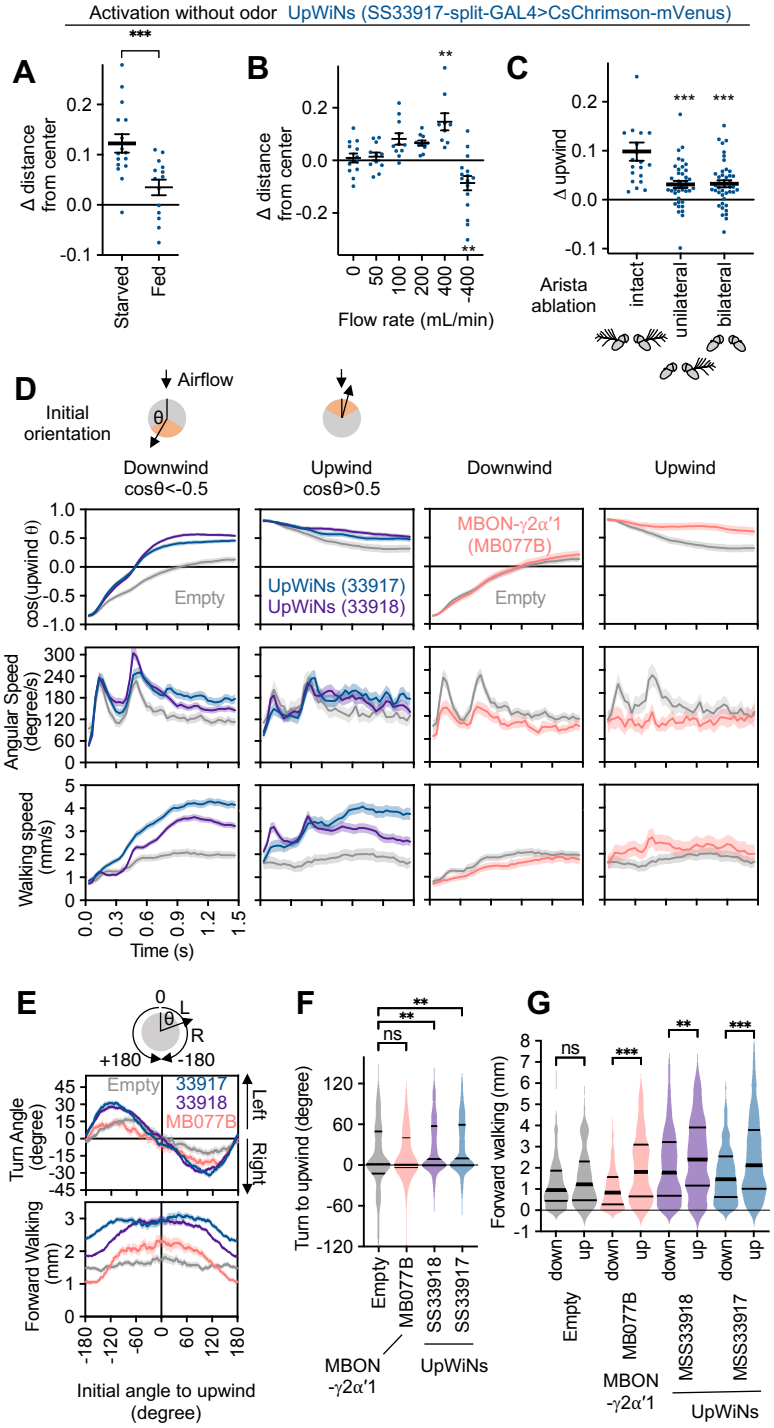
Activation without odor UpWiNs (SS33917-split-GAL4>CsChrimson-mVenus)
A
Δ distance from center
Starved
Fed
B
Δ distance from center
Flow rate (mL/min)
C
Δ upwind
Arista ablation
intact
unilateral
bilateral
D
Airflow
Initial orientation
Downwind cosθ<-0.5
Upwind cosθ>0.5
Downwind
Upwind
cos(upwind θ)
Empty
UpWiNs (33917)
UpWiNs (33918)
MBON-γ2α′1 (MB077B)
Angular Speed (degree/s)
Walking speed (mm/s)
Time (s)
E
Turn Angle (degree)
Forward Walking (mm)
Empty
33917
33918
MB077B
Left
Right
Initial angle to upwind (degree)
F
Turn to upwind (degree)
Empty
MB077B
SS33918
SS33917
MBON -γ2α′1
UpWiNs
G
Forward walking (mm)
down
up
Empty
MB077B
MSS33918
MSS33917
MBON -γ2α′1
UpWiNs

Figure 6

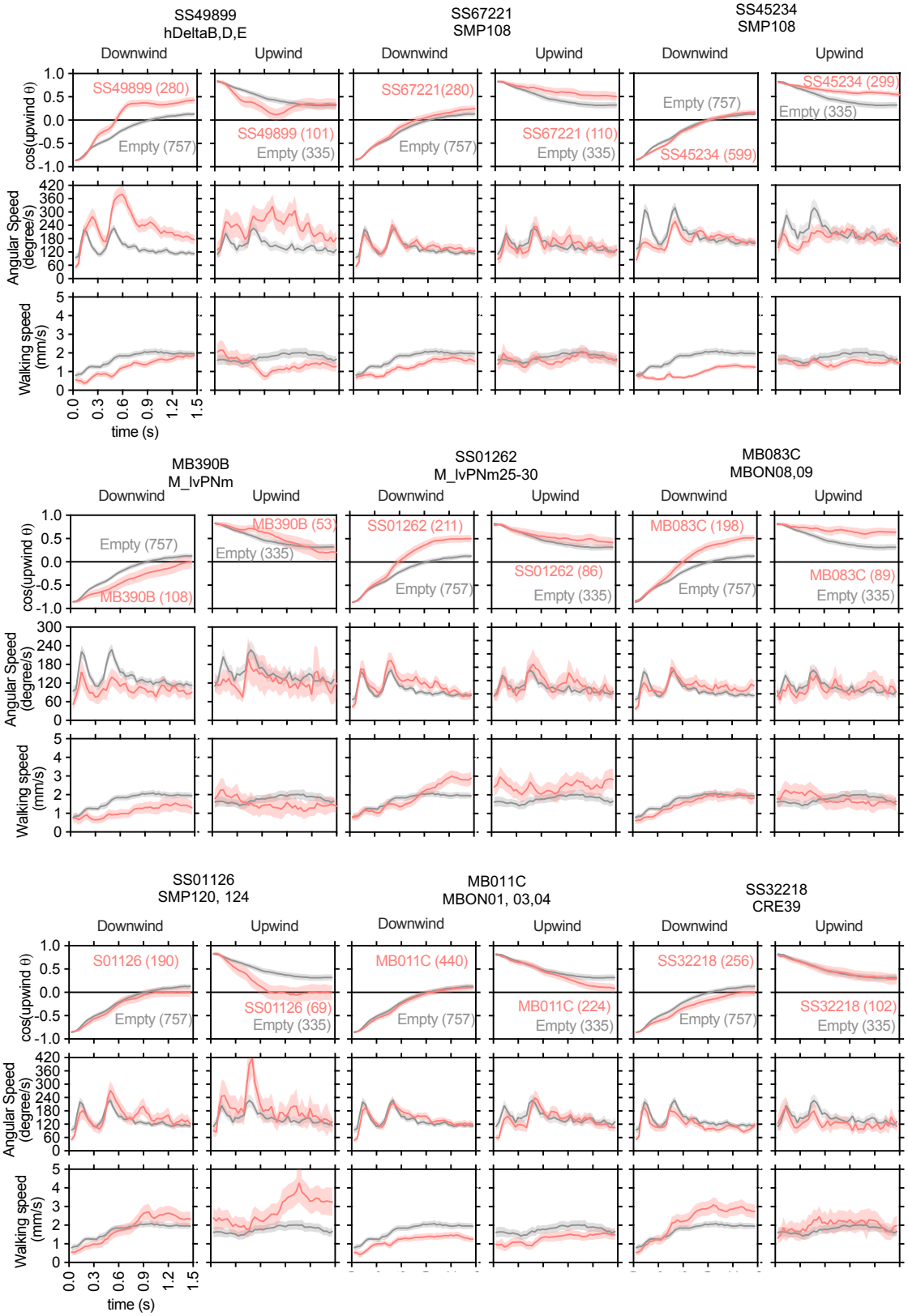

Figure 6-figure Supplement 1

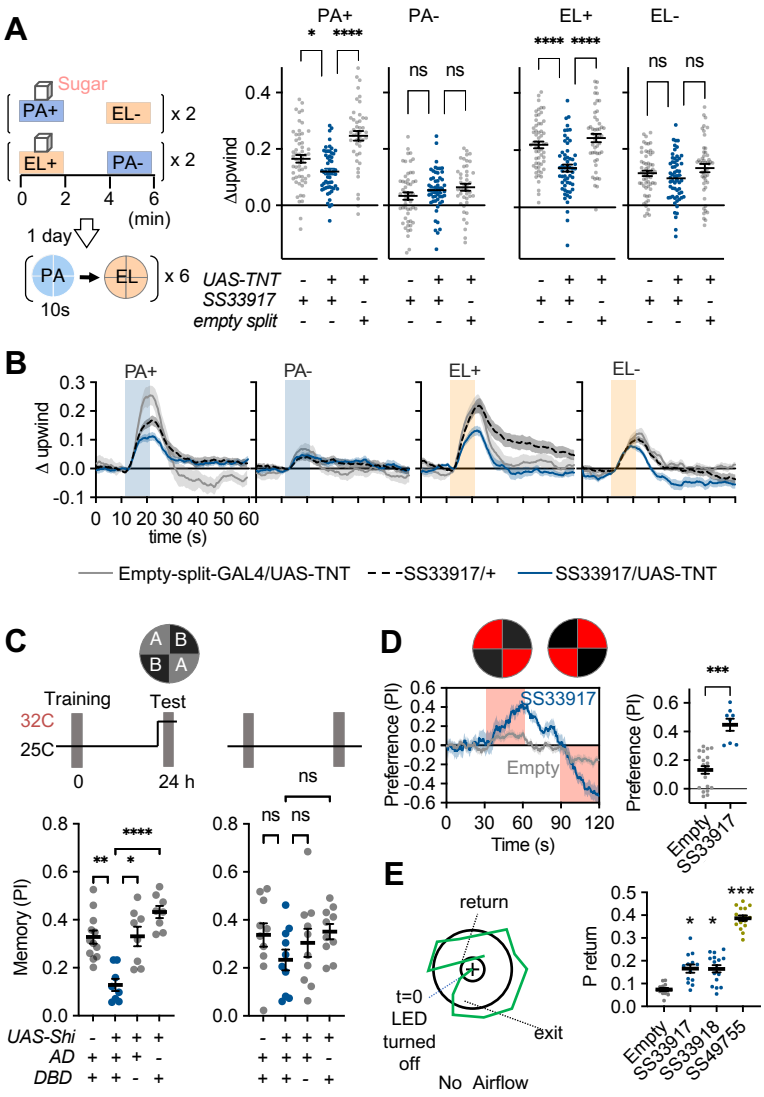
A
Sugar
PA+
EL-
x 2
EL+
PA-
x 2
0 2 4 6
(min)
1 day
PA
EL
x 6
10s
PA+
PA-
EL+
EL-
Δupwind
UAS-TNT
SS33917
empty split
B
PA+
PA-
EL+
EL-
Δ upwind
time (s)
Empty-split-GAL4/UAS-TNT
SS33917/+
SS33917/UAS-TNT
C
A B
B A
Training
Test
32C
25C
0
24 h
ns
Memory (PI)
UAS-Shi
AD
DBD
D
SS33917
Empty
Preference (PI)
Time (s)
Preference (PI)
Empty
SS33917
E
return
t=0
LED
turned
off
exit
No Airflow
P return
Empty
SS33917
SS33918
SS49755

Figure 7

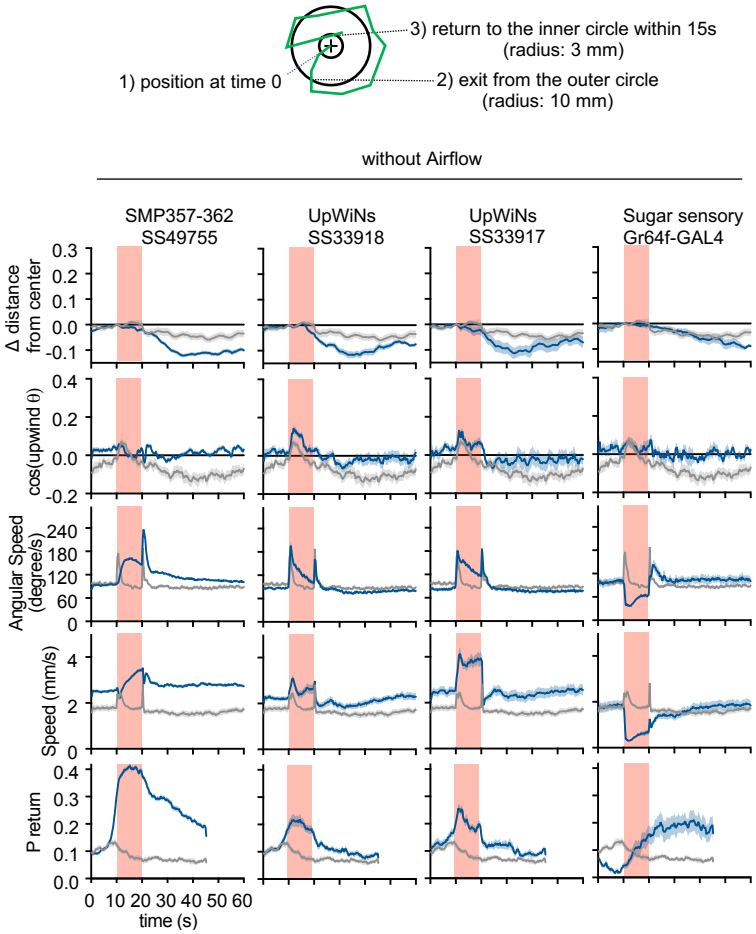

Figure 7-figure supplement 1